Measures of Cosmic Structure

Lecture course LSS2009
University Groningen
Apr. 2009-July 2009

Standard Reference:

Martinez & Saar

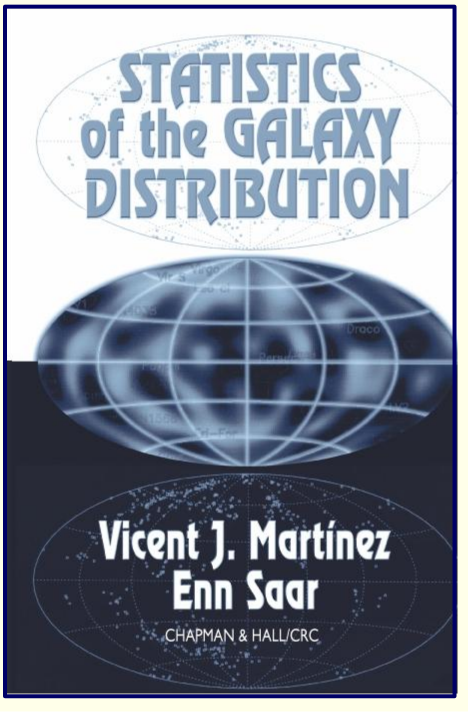

Ergodic Theorem

Statistical Cosmological Principle

Cosmological Principle:

Universe is Isotropic and Homogeneous

Homogeneous & Isotropic Random Field $\psi(\vec{x})$:

Homogenous $\quad p[\psi(\vec{x}+\vec{a})] = p[\psi(\vec{x})]$

Isotropic $\quad p[\psi(\vec{x}-\vec{y})] = p[\psi(|\vec{x}-\vec{y}|)]$

Within Universe <u>one</u> particular <u>realization</u> $\psi(\vec{x})$:

<u>Observations</u>: only spatial distribution in that one particular $\psi(\vec{x})$

<u>Theory</u>: $p[\psi(\vec{x})]$

Ergodic Theorem

Ensemble Averages	$\Longleftrightarrow$	**Spatial Averages over one realization of random field**

• Basis for statistical analysis cosmological large scale structure

• In statistical mechanics Ergodic Hypothesis usually refers to time evolution of system, in cosmological applications to <u>spatial distribution</u> at one fixed time

Ergodic Theorem

Validity Ergodic Theorem:

• Proven for Gaussian random fields with continuous power spectrum

• Requirement:

spatial correlations decay sufficiently rapidly with separation

such that

<u>many statistically independent volumes</u> in one realization

$\Downarrow$

All information present in complete distribution function $p[\psi(\vec{x})]$ available from single sample $\psi(\vec{x})$ over all space

Fair Sample Hypothesis

- Statistical Cosmological Principle

+

- Weak cosmological principle
  (small fluctuations initially and today over Hubble scale)

+

- Ergodic Hypothesis

fair sample hypothesis
(Peebles 1980)

Discrete e.g. Continuous

Discrete & Continuous Distributions

- How to relate discrete and continuous distributions:
- Define number density $n(\vec{x})$ for a point process:

$$\boxed{n(\vec{x}) = \bar{n}[1+\delta(\vec{x})] = \sum_i \delta_D(\vec{x}-\vec{x}_i)}$$

$\delta_D(\vec{x})$ Dirac Delta function

$\left\langle \sum_i \delta_D(\vec{x}-\vec{x}_i) \right\rangle = \bar{n}$ ensemble average

Correlation Functions

Correlation Functions

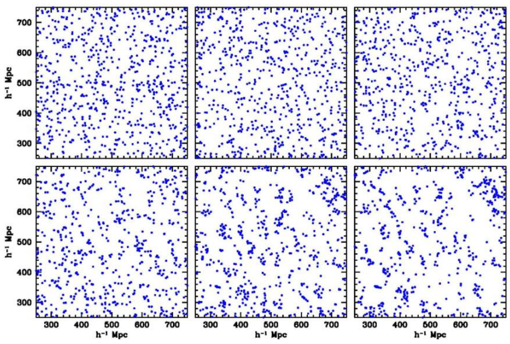

Joint probability that in each one of

the two infinitesimal volumes dV_1 & dV_2,

at distance r,

lies a galaxy

Infinitesimal Definition Two-Point Correlation Function:

$$dP(r) = \bar{n}^2 \, (1 + \xi(r)) \, dV_1 dV_2$$

mean density

Correlation Functions

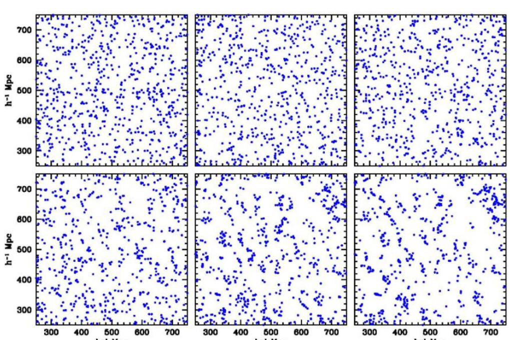

In case of Homogeneous & Isotropic point process

then $\xi(\vec{r})$

only dependent on

$|\vec{r}| = r$

Infinitesimal Definition Two-Point Correlation Function:

$$dP(r) = \bar{n}^2 \, (1 + \xi(r)) \, dV_1 dV_2$$

mean density

Correlation Functions

Discrete $\Longleftrightarrow$ Continuous

<u>Two-point correlation function</u>

$$dP(\vec{x}_1, \vec{x}_2) = \bar{n}^2 dV_1 dV_2 [1 + \xi(r_{12})]$$

$$r_{12} = |\vec{x}_1 - \vec{x}_2|$$

$$\langle \delta(\vec{x}) \rangle = 0$$

<u>Autocorrelation function</u>

$$\xi(r_{12}) = \langle \delta(\vec{x}_1) \delta(\vec{x}_2) \rangle$$

probability for 2 points in dV_1 and dV_2

Correlation Functions

- Gaussian (primordial and large-scale) density field:

  Autocorrelation function ξ(r) Fourier transform power spectrum P(k)

  $$\xi(\mathbf{r}) = \xi(|\mathbf{r}|) = \int \frac{\mathrm{d}\mathbf{k}}{(2\pi)^3} P_f(k) \mathrm{e}^{-\mathrm{i}\mathbf{k}\cdot\mathbf{r}}$$

  Autocorrelation function completely specifies statistical properties of field

- First order measure of deviations from uniformity

- Nonlinear objects (halos):
  ξ(r) measure of density profile

- Large Scales:
  related to dynamics of structure formation via e.g. cosmic virial theorem

Correlation Functions:
related measures

Other measures related to $\xi(r)$:

- Second-order intensity $\lambda_2(r) = \bar{n}^2 \xi(r) + 1$
- Pair correlation function $g(r) = 1 + \xi(r)$
- Conditional density $\Gamma(r) = \bar{n}(1 + \xi(r))$

Correlation Functions:
related measures

$$J_3(r) \equiv \int_0^\infty \xi(y) y^2 dy$$

Volume averaged correlation function $\bar{\xi}(r)$

$$\bar{\xi}(r) = \frac{3}{4\pi r^3} \int_0^r 4\pi \xi(x) x^2 dx = \frac{3 J_3(r)}{r^3}$$

Power-law Correlations

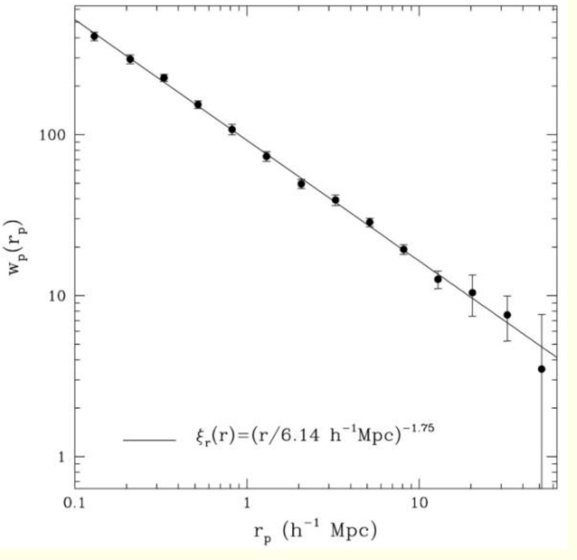

$$\xi(r) = \left(\frac{r}{r_0}\right)^{-\gamma}$$

$$\gamma \approx 1.8$$

$$r_0 \approx 5h^{-1}Mpc$$

Totsuji & Kihara 1969

Peebles 1975, 1980, …

Correlation Functions

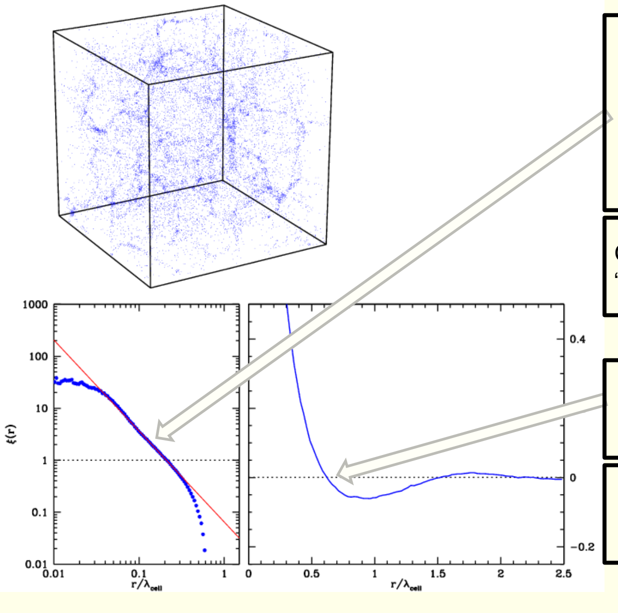

$$\xi_{cc}(r) = \left(\frac{r_o}{r}\right)^{\gamma}$$

$$\xi(r_o) = 1 .$$

Clustering length/
“Correlation” length

Coherence length

$$\xi(r_a) = 0$$

Correlation Function Estimators

Minimal Estimator

$$\hat{\xi}_{\min}(r) = \frac{V(W)}{NN_{in}} \sum_{i=1}^{N_{in}} \frac{n_i(r)}{V_{sh}} - 1$$

For galaxies close to the boundary the number of neighbours is Underestimated. One way to overcome this problem is to consider as centers for counting neighbours only galaxies lying within an inner window W_{in}

V_{sh} is the volume of the shell of width dr

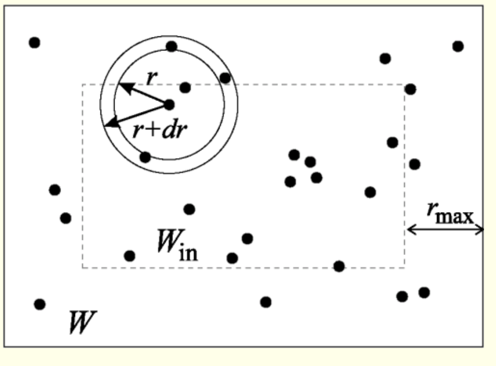

Edge-Corrected Estimator

$$\hat{\xi}_{edge}(r) = \frac{V(W)}{N^2} \sum_{i=1}^{N_{in}} \frac{n_i(r)}{V_i} - 1$$

$N_i(r)$: number of neighours at distance in the interval [r,r+dr] from galaxy I

V_i: volume of the intersection of the shell with W

W: when W a cube, an analytic expression for V_i can be found in Baddely et al. (1993).

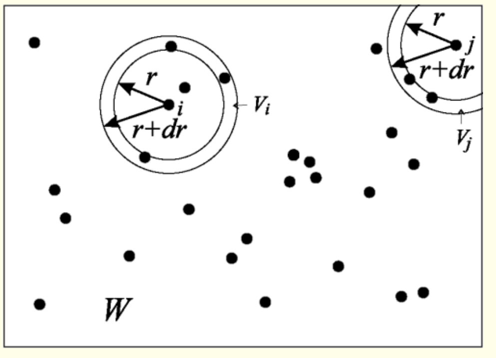

Estimators Redshift Surveys

- In redshift surveys, galaxies are not sampled uniformly over the survey volume
- Depth selection:
  in magnitude-limited surveys, the sampling density decreases as function of distance
- Survey Geometry
  boundaries of survey often nontrivially defined:
  - slice surveys
  - non-uniform sky coverage
  etc.

⇩

Clustering in survey compared with sample of Poisson distributed points, following the same sampling behaviour in depth and survey geometry

Difference in clustering between
data sample (D) and Poisson sample (R)
genuine clustering

Estimators Redshift Surveys

Clustering in survey compared with sample of Poisson distributed points, following the same sampling behaviour in depth and survey geometry

Difference in clustering between
data sample (D) and Poisson sample (R)
genuine clustering

- $$\xi_{DP}(r) = \frac{n_R}{n_D} \frac{\langle DD \rangle}{\langle RR \rangle} - 1$$ Davis-Peebles (1983)
- $$\xi_{Ham}(r) = \frac{\langle DD \rangle \langle RR \rangle}{\langle DR \rangle^2} - 1$$ Hamilton (1993)
- $$\xi_{LS}(r) = 1 + \left(\frac{n_R}{n_D} \right)^2 \frac{\langle DD \rangle}{\langle RR \rangle} - 2 \frac{n_R}{n_D} \frac{\langle DR \rangle}{\langle RR \rangle}$$ Landy-Szalay (1993)

Angular
Two-point Correlation Function

Angular Correlation Function

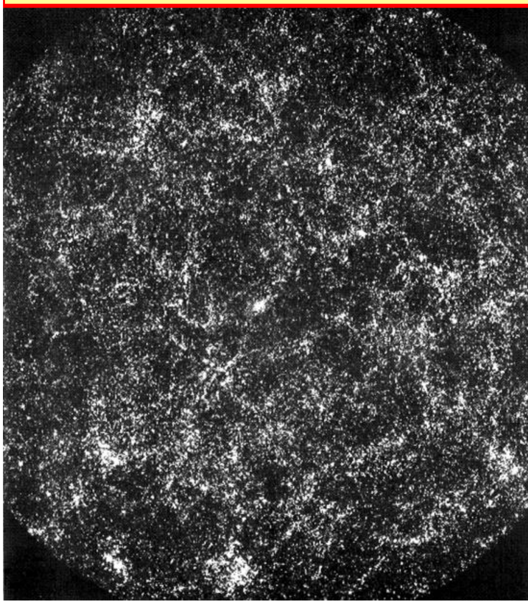

Galaxy sky distribution:

- Galaxies clustered, a projected expression of the true 3-D clustering
- Probability to find a galaxy near another galaxy higher than average (Poisson) probability
- Quantitatively expressed by 2-pt correlation function w(θ):

$$\boxed{dP(\theta) = \bar{n}^2 \{1 + w(\theta)\} d\Omega_1 d\Omega_2}$$

Excess probability of finding 2 gal's at angular distance θ

Angular & Spatial Clustering

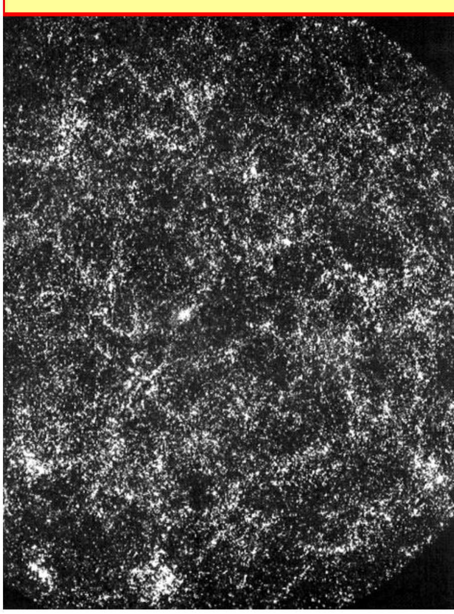

$$\boxed{dP(\theta) = \bar{n}^2 \{1 + w(\theta)\} d\Omega_1 d\Omega_2}$$

$$\Downarrow$$

Two-point angular correlation function is the "projection" of $\xi(r)$

Limber's Equation:

$$\boxed{w(\theta) = \frac{\iint p(\vec{x}_1)\, p(\vec{x}_2)\, x_1^{\,2} x_2^{\,2}\, dx_1 dx_2\, \xi(|\vec{x}_1 - \vec{x}_2|)}{\left[\int_0^\infty x^2 p(x) dx\right]^2}}$$

p(x): survey selection function

Limber Equation

$$w(\theta) = \frac{\iint p(\overrightarrow{x_1})\, p(\overrightarrow{x_2})\, {x_1}^2 {x_2}^2 dx_1 dx_2 \xi(|\overrightarrow{x_1} - \overrightarrow{x_2}|)}{\left[\int_0^\infty x^2 p(x) dx\right]^2}$$

$$\Downarrow$$

$$\xi(r) = \left(\frac{r_0}{r}\right)^\gamma \quad \longleftrightarrow \quad w(\theta) = A\left(\frac{1}{\theta}\right)^{\gamma-1}$$

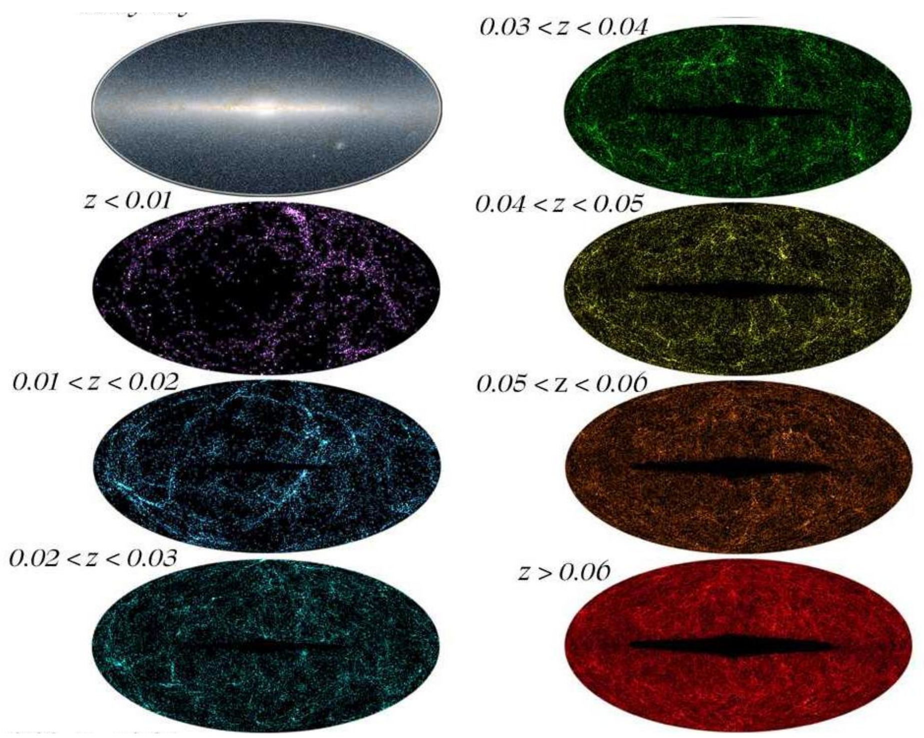

Angular Clustering Scaling

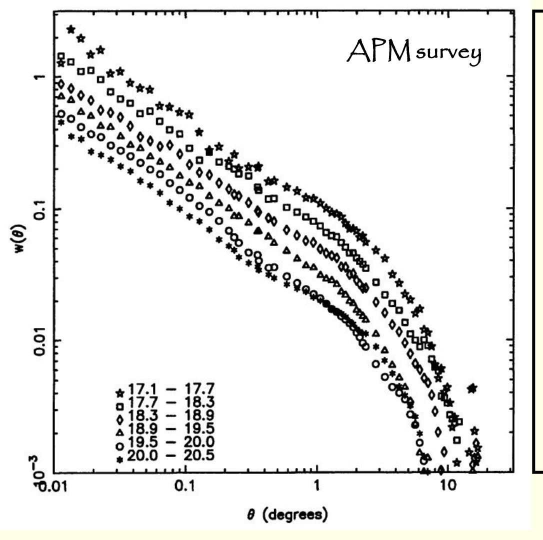

Two-point correlation function:

- small angles: power-law

$$w(\theta) = \left(\frac{\theta_0}{\theta}\right)^{\gamma}$$

$$\gamma \approx 0.8$$

- large angles ⟶ 0

ie. to homogeneity

Angular Clustering Scaling

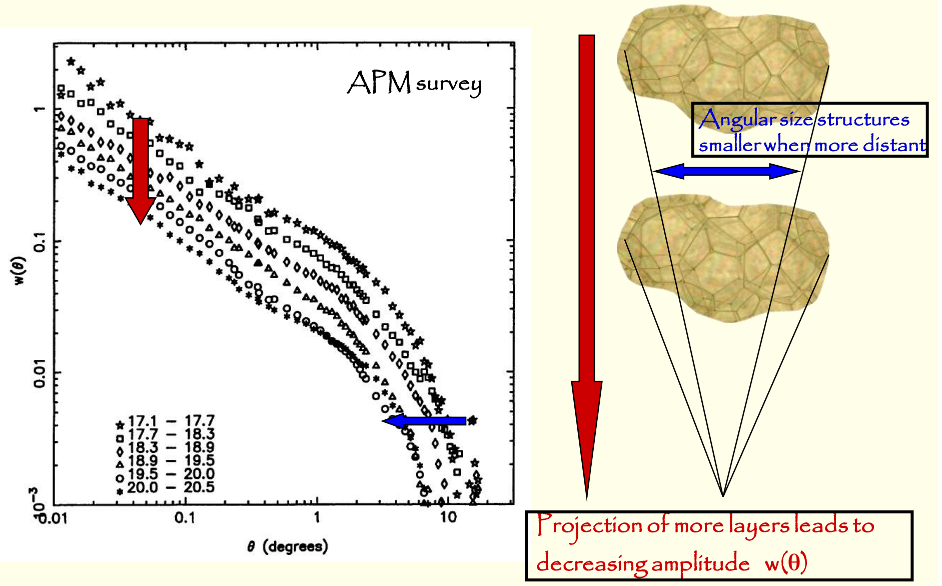

Projection of more layers leads to decreasing amplitude w(θ)

Angular Clustering Scaling

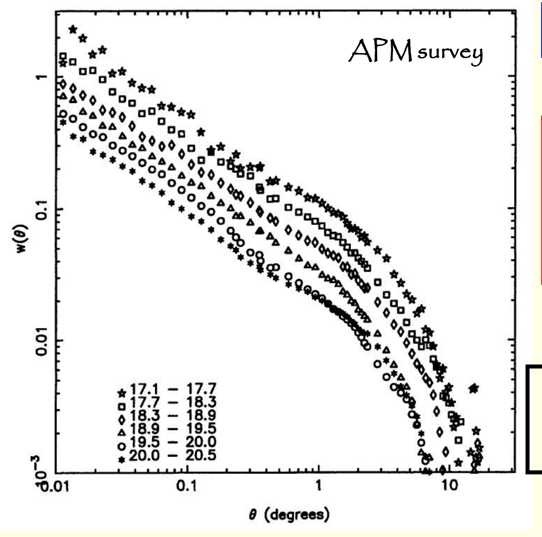

Angular size structures smaller when more distant

Projection of more layers leads to decreasing amplitude w(θ)

$$w(\theta, D_*) = \frac{1}{D_*} w(\theta D_*)$$

Angular Clustering Scaling

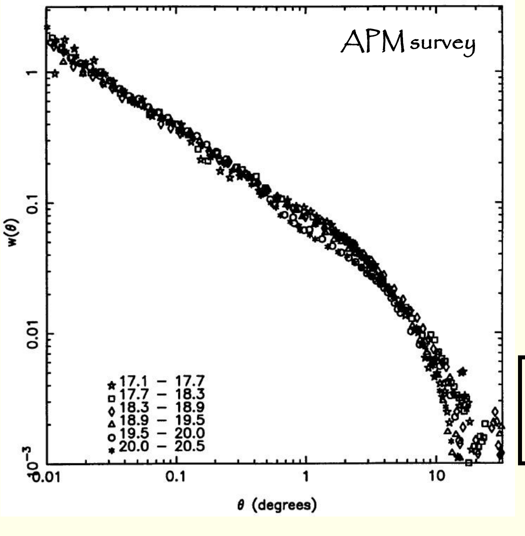

Angular size structures smaller when more distant

Projection of more layers leads to decreasing amplitude w(θ)

$$w(\theta, D_*) = \frac{1}{D_*} w(\theta D_*)$$

Angular Clustering Scaling

The angular scaling of $w(\theta)$ is found back to even fainter magnitudes in the SDSS survey (m=22)

Clear evidence that there are no significant large structures on scales > 100-200 Mpc

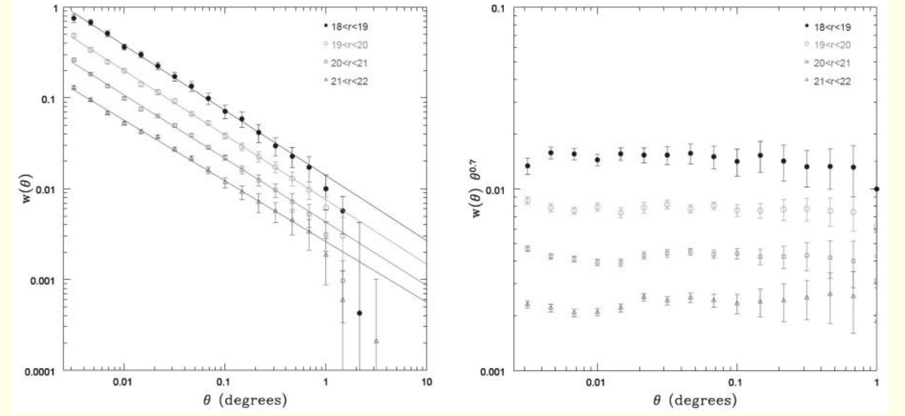

Redshift Space Distortions

Redshift Distortions

- In reality, galaxies do not exactly follow the Hubble flow:

  In addition to the cosmological flow, there are locally induced velocity components in a galaxy's motion:

$$cz = Hr + v_{pec}$$

  the galaxy's peculiar velocity v_{pec}

- As a result, maps on the basis of galaxy z do not reflect the galaxies' true spatial distribution

Redshift Distortions

Origin of peculiar velocities:

three regimes

- very high-density virialized cluster (core) regions:
  "thermal" motion in cluster,
  up to > 1000 km/s

  "Fingers of God"

- collapsing overdensity (forming cluster):
  inflow/infall velocity

- Large scales:
  (linear, quasi-linear) cosmic flow,
  manifestation of structure growth

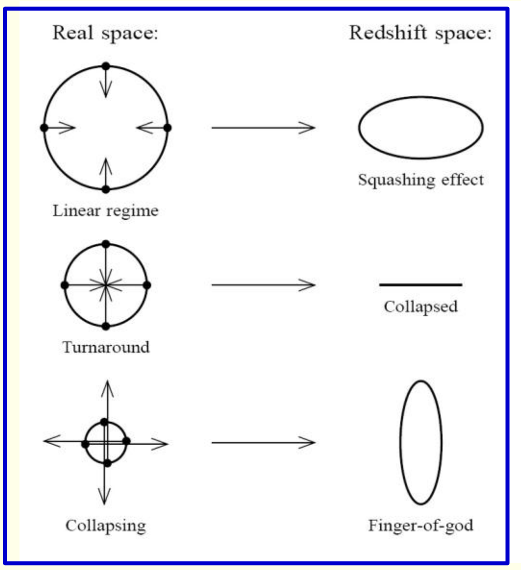

Fingers of God

$$cz = Hr_{clust} + \frac{\vec{v}_{gal} \cdot \vec{r}_{gal}}{r_{gal}}$$

Galaxy velocity component along line of sight

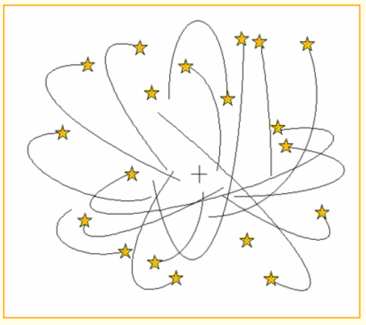

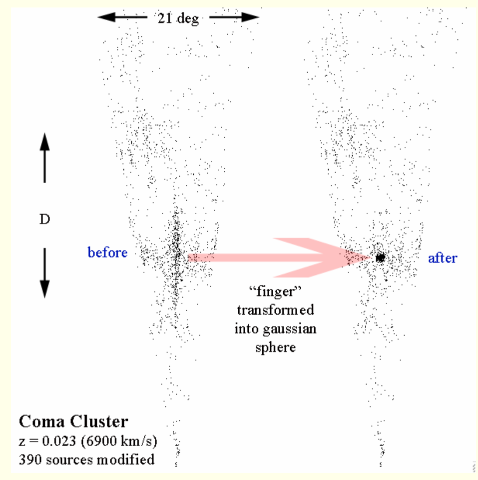

Fingers of God

Clusters of galaxies:

Mass: 10^{14}-$10^{15}\,M_\odot$
Radius: ~ 1.5 Mpc
Overdensity Δ ~ 1000

Thermal velocity: ~ 1000 km/s

Internal cluster galaxy velocities visible in projection along line of sight

→ "Finger of God"

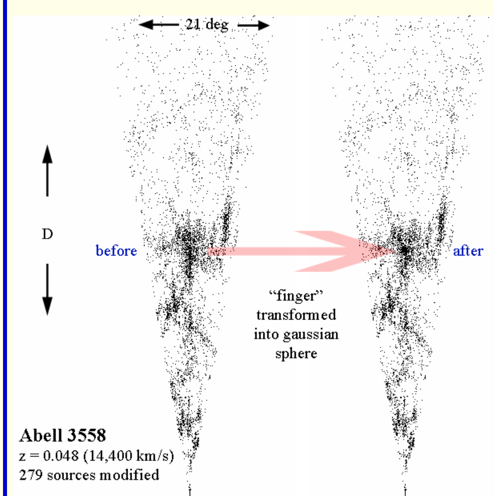

Nonlinear Infall Pattern

Cluster Infall:

Matter in surroundings falling in onto cluster:

- infall velocities up to 1000 km/s radially declining:
- velocities decrease as distance to cluster centre increases
- projected radial velocity function of angle & distance wrt. cluster centre.

→

- triple-value region redshift space:
  - within turnaround radius, a particular redshift z may correspond to 3 spatial positions

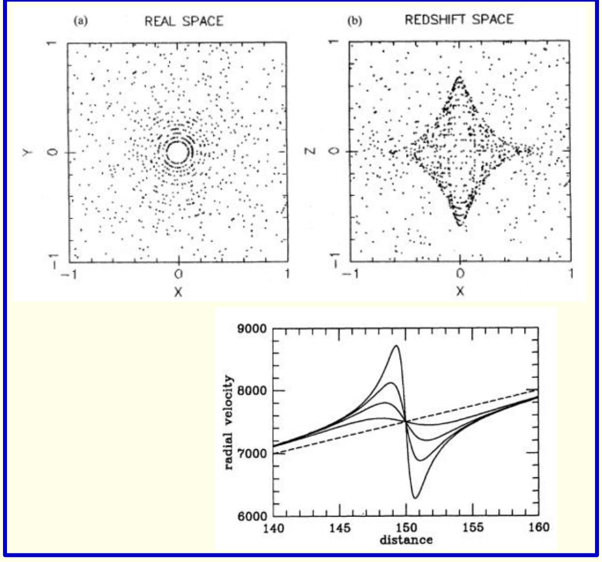

Nonlinear Infall Pattern

Cluster Caustics:

Three-value region cluster infall:

Projection onto restricted cone-shaped redshift space regions around clusters

Enclosed within caustic surfaces

Position caustics dependent on Ω_m

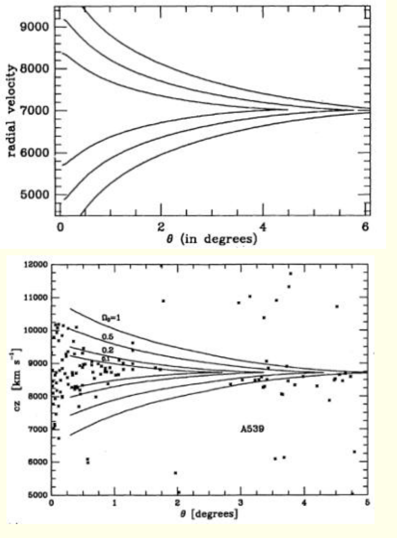

Large Scale Flows

Large-Scale Flows:

- On large (Mpc) scales, structure formation still in linear regime
- Structure buildup accompanied by displacement of matter: - Cosmic flows
- Directly related to cosmic matter distribution
- In principle possible to correct for this distortion, ie. to invert the mapping from real to redshift space
- Condition: entire mass distribution within volume should be mapped

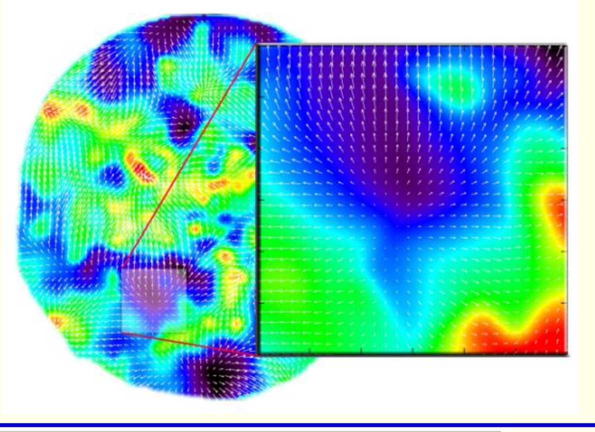

$$\mathbf{v}(\mathbf{x},t) = \frac{H}{4\pi}\frac{f(\Omega_m)}{b}\,a\int d\mathbf{x}'\,\delta_{gal}(\mathbf{x}',t)\,\frac{(\mathbf{x}'-\mathbf{x})}{|\mathbf{x}'-\mathbf{x}|^3}$$

Large Scale Flows

Large-Scale Flows:

The induced large scale peculiar velocities translate into extra contributions to the redshift of the galaxies

Compare "real space" structure vs. "redshift space" structure

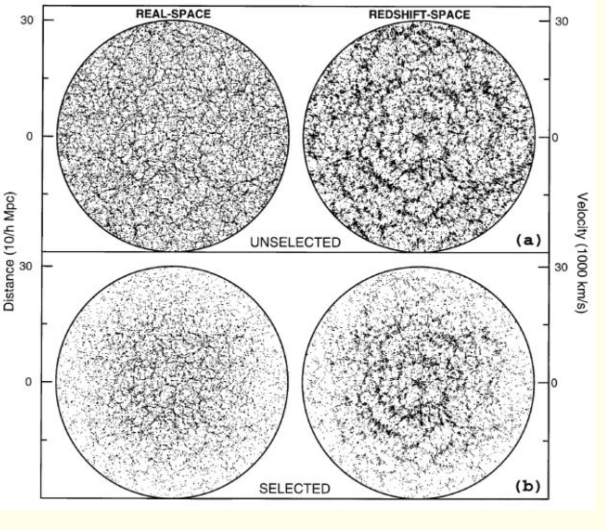

Correlation Functions:

Redshift Space

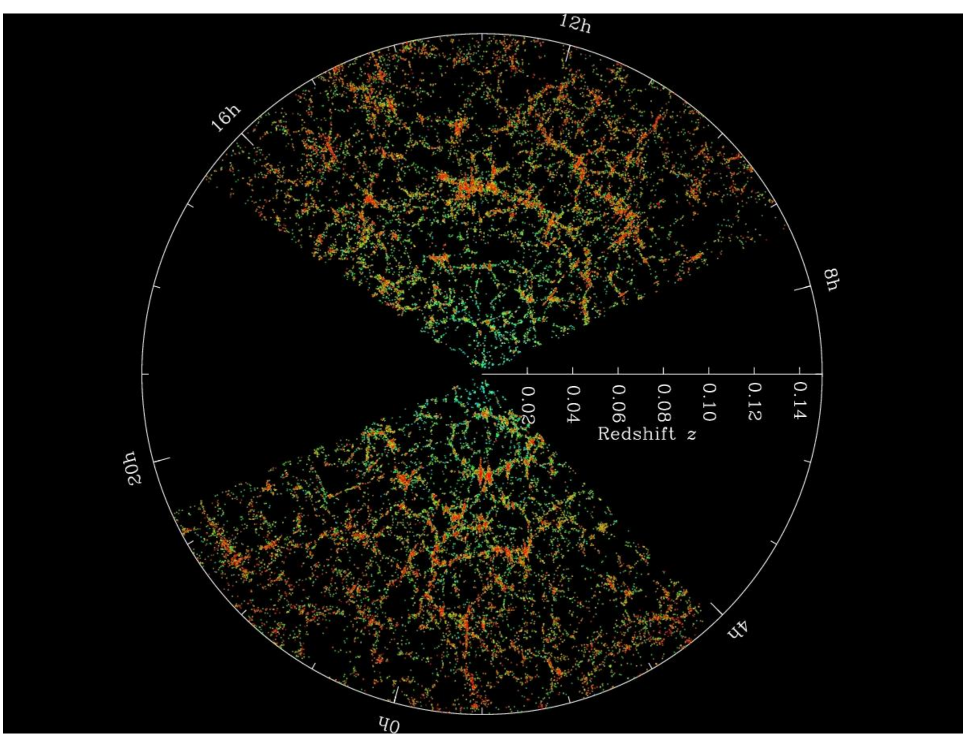

sky-redshift space 2-pt correlation function $\xi(\sigma,\pi)$

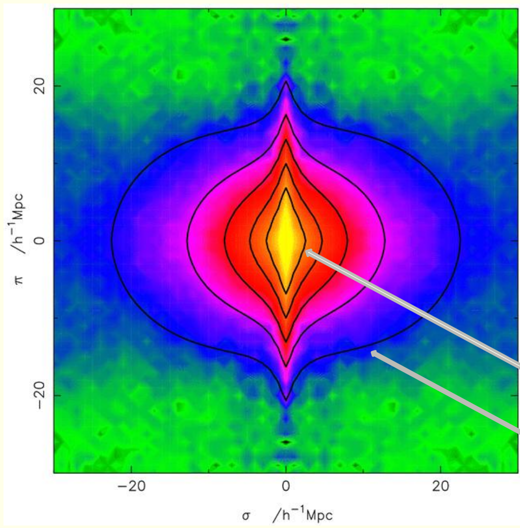

Correlation function determined in sky-redshift space:

$$\boxed{\xi(\sigma,\pi)}$$

sky position: $\sigma = (\alpha, \delta)$

redshift coordinate: $\pi = cz$

Close distances:
distortion due to non-linear Finger of God

Large distances:
distortions due to large-scale flows

Redshift Space Distortions Correlation Function

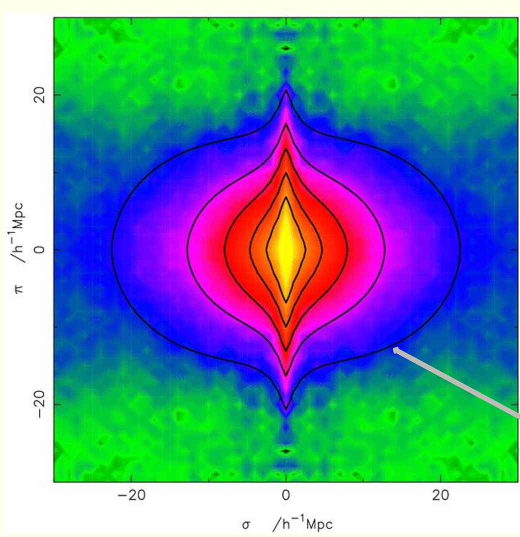

On average, $\xi_s(s)$ gets amplified wrt. $\xi_r(r)$

Linear perturbation theory (Kaiser 1987):

$$\boxed{\xi_s(s) = (1 + \frac{2}{3}\Omega^{0.6} + \frac{1}{5}\Omega^{1.2})\xi_r(s)}$$

Large distances:
distortions due to large-scale flows

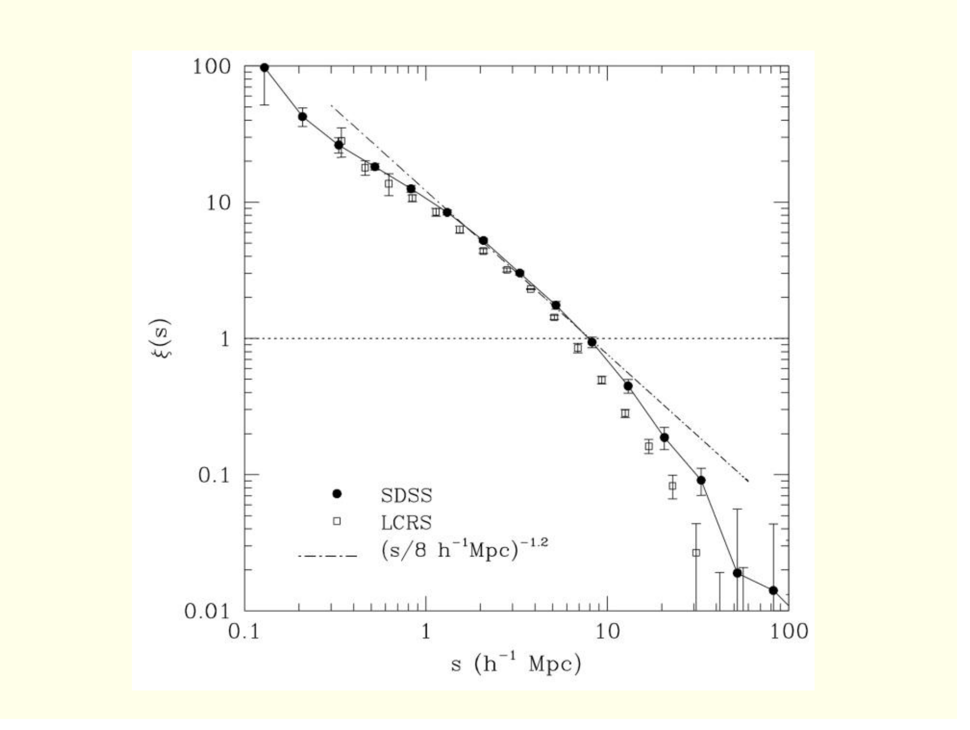

100
10
1
0.1
0.01
ξ(s)
0.1
1
10
100
s (h^{-1} Mpc)
SDSS
LCRS
(s/8 h^{-1}Mpc)$^{-1.2}$

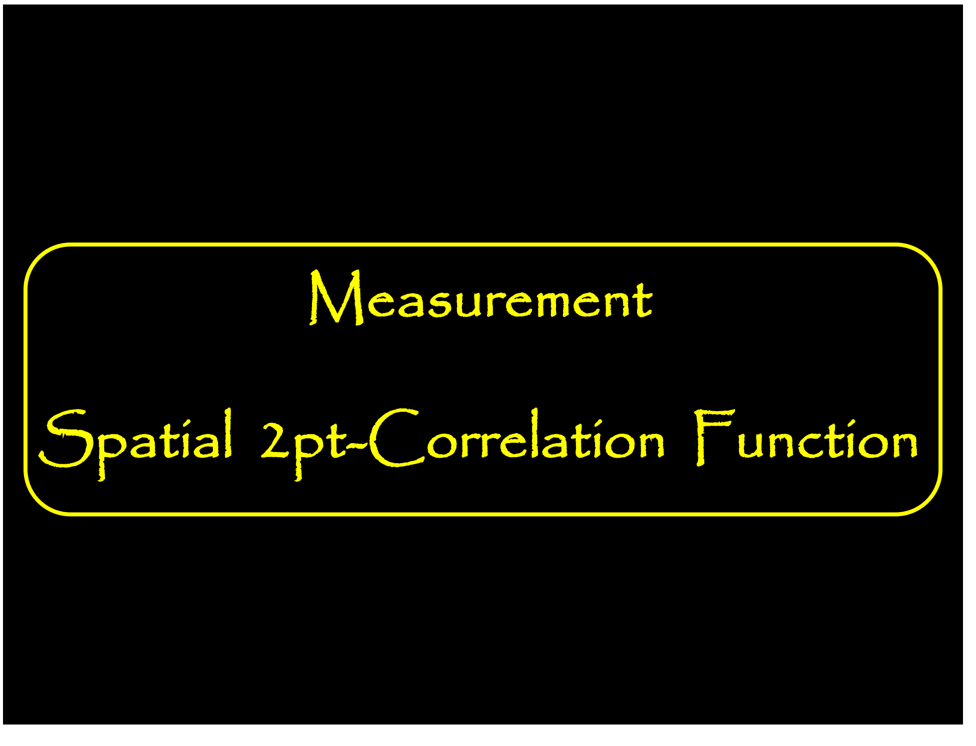

Measurement
Spatial 2pt-Correlation Function

Deprojected Spatial Correlations

2pt correlation function
not an ideal power-law:

Halo Model:

Two-point correlation function combination of

1) small-scale correlations, due to galaxies inside one dark matter halo

2) large scale correlations between dark matter halos

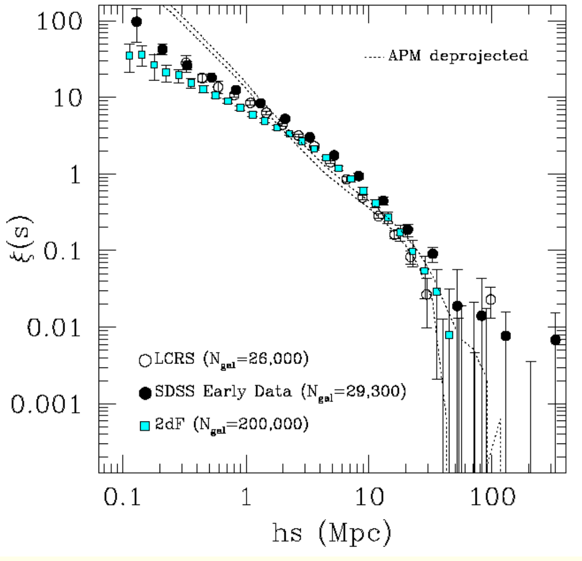

Convergence to Homogeneity

The correlation function g(r)=1+ξ(r)

Stromlo-APM, Las Campanas CfA2, ESP redshift surveys.

The fractal behavior at small scales dissapears at larger distances, providing evidence for a gradual transition to homogeneity.

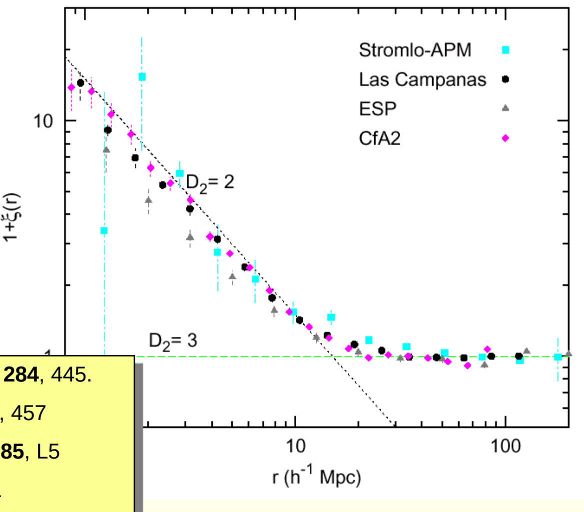

Plot from Martínez, 1999, Science, **284**, 445.

(1) Loveday *et al.*, 1995, ApJ, **442**, 457

(2) Tucker *et al.*, 1997, MNRAS, **285**, L5

(3) Guzzo *et al.*, 2000, AA, **355**, 1

Luminosity Dependence Correlation Functions

Galaxy Luminosity Dependence

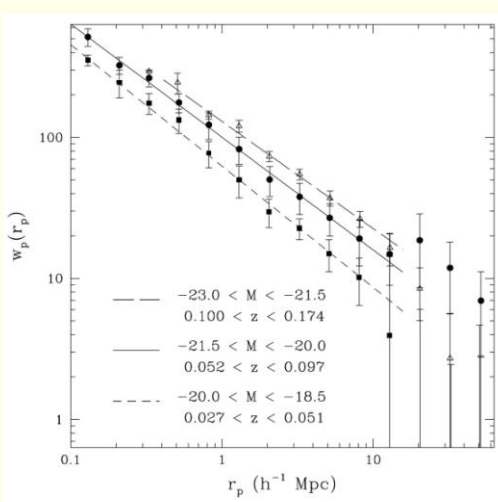

SDSS
correlation function

for galaxies in different
luminosity bins

Spatial Structure &

Correlation Functions

Structural Insensitivity

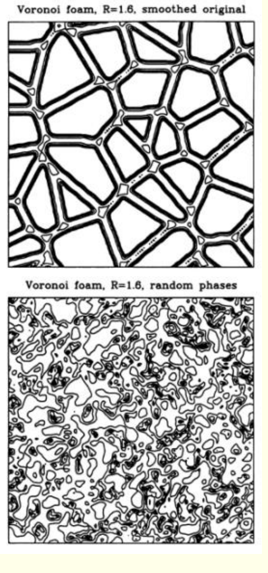

2-pt correlation function is
highly insensitive to the geometry & morphology
of weblike patterns:

> compare 2 distributions with same
> $\xi(r)$, cq. P(k),
> but totally different phase distribution

In practice, some sensitivity in terms of distinction
Field, Filamentary, Wall-like and Cluster-dominated
distributions:

because of different fractal dimensions

Structural Sensitivity

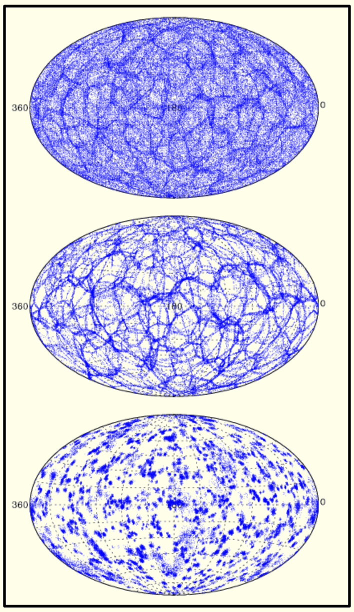

Wall-dominated

Filamentary

Cluster-like

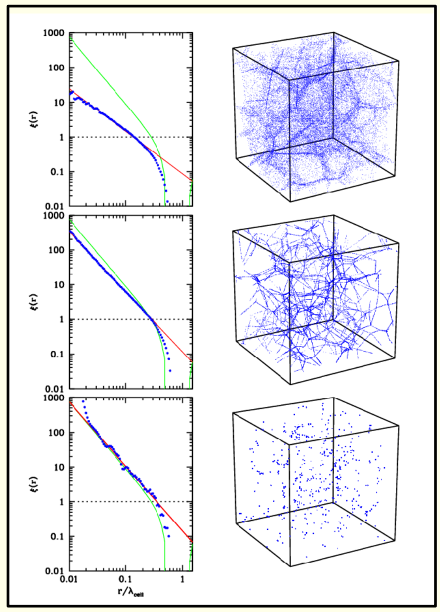

Cluster

Correlation Functions

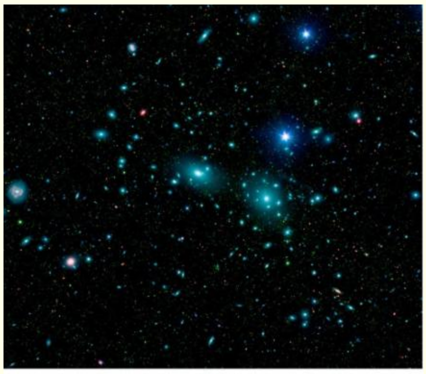

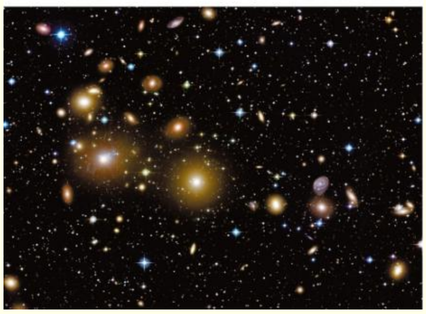

Clusters of Galaxies

Coma Cluster

Perseus Cluster

Clustering of Clusters

Clusters cluster much more strongly than galaxies:

- clustering defines superclusters !
- also power-law 2-pt correlation fct.
- same power law slope $\gamma \sim 1.8$
- much higher correlation length r_0 :

$r_0 \sim$ 15-25 h^{-1} Mpc

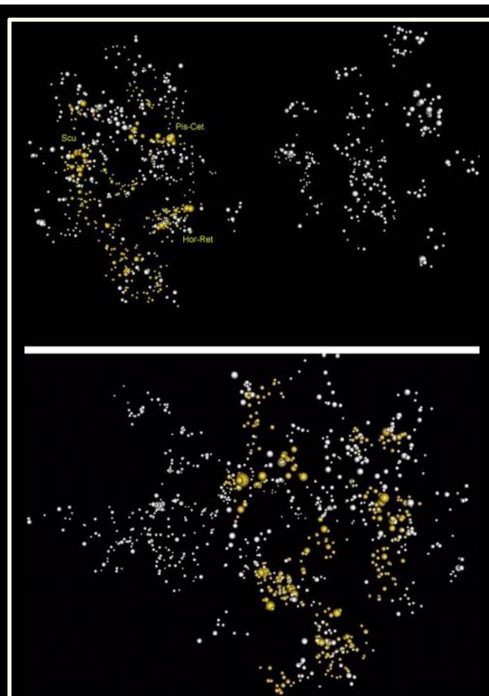

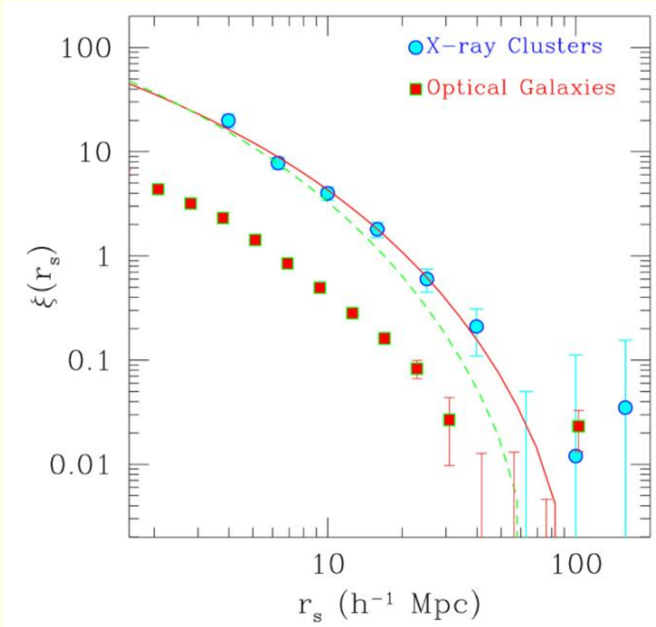

Richness-Dependent Cluster Correlations

More massive clusters are systematically more strongly clustered than lower mass ones.

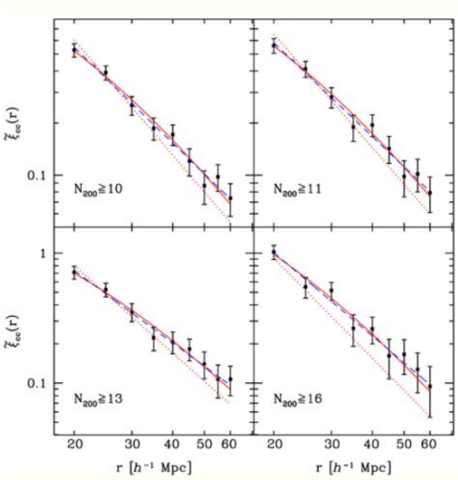

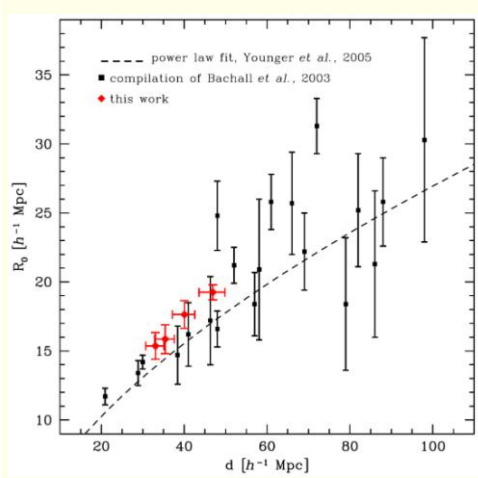

Richness-Dependent Cluster Correlations

More massive clusters are more systematically more strongly clustered than lower mass ones:

simple model:
Szalay & Schramm 1985

$$\xi_{cc}(r) = \beta \left(\frac{L(r)}{r} \right)^{\gamma}$$

$$L(R) = n^{-1/3}$$

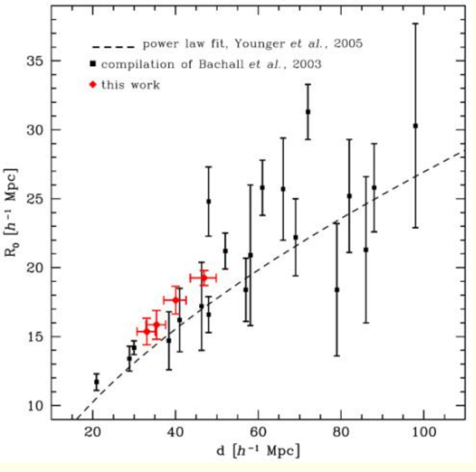

Scaling of Cluster Correlation Functions: a geometric model

Voronoi Models:

Templates for the Cosmic Web

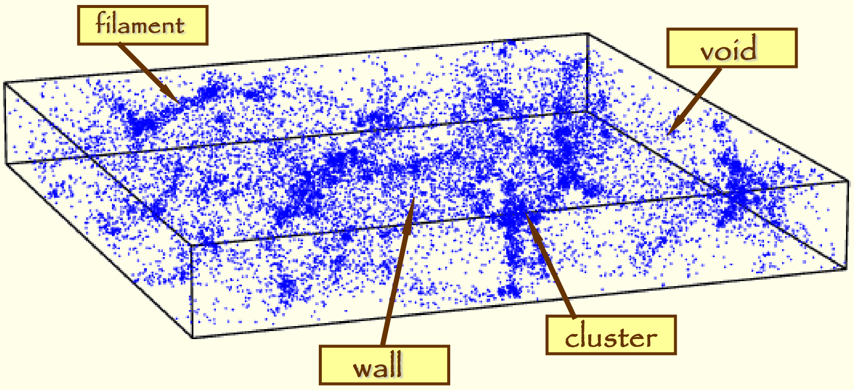

Perfect
Power-law clustering
Voronoi vertices

$$\xi_{vv}(r) = \left(\frac{r_0}{r}\right)^{\gamma}$$

$$\gamma = 1.95; \qquad r_0 \approx 0.3\,\lambda_c$$

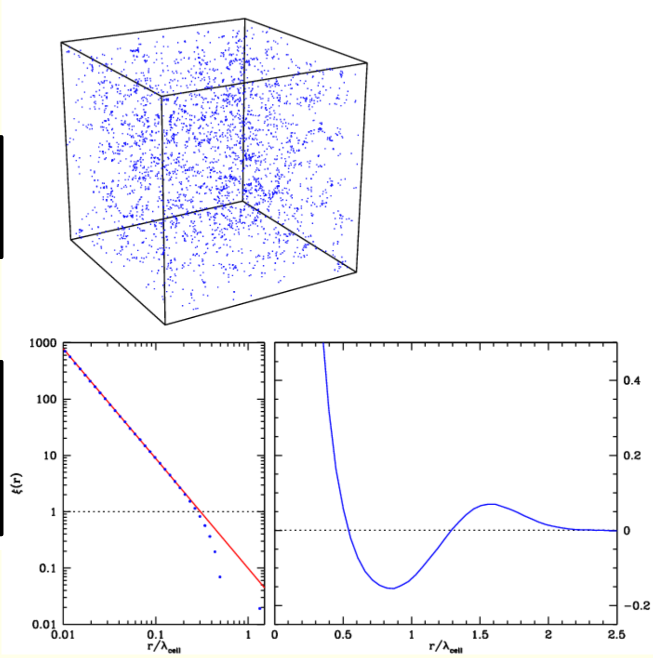

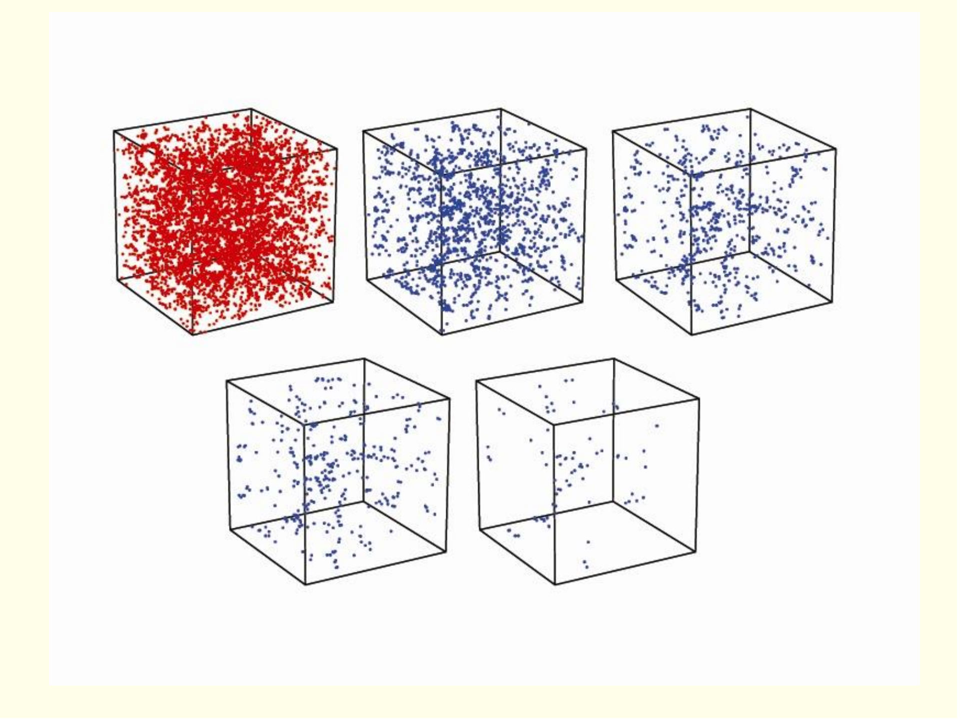

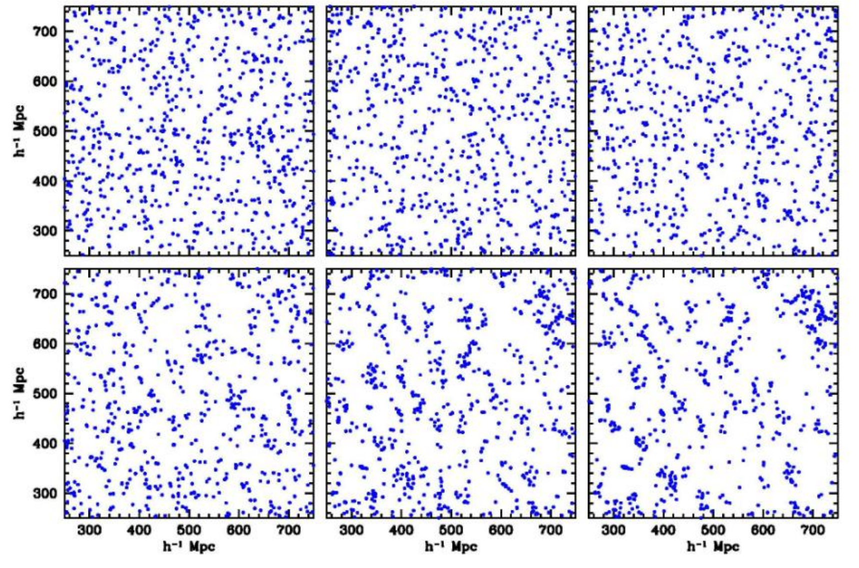
h⁻¹ Mpc
300
400
500
600
700

Self-similar Clustering

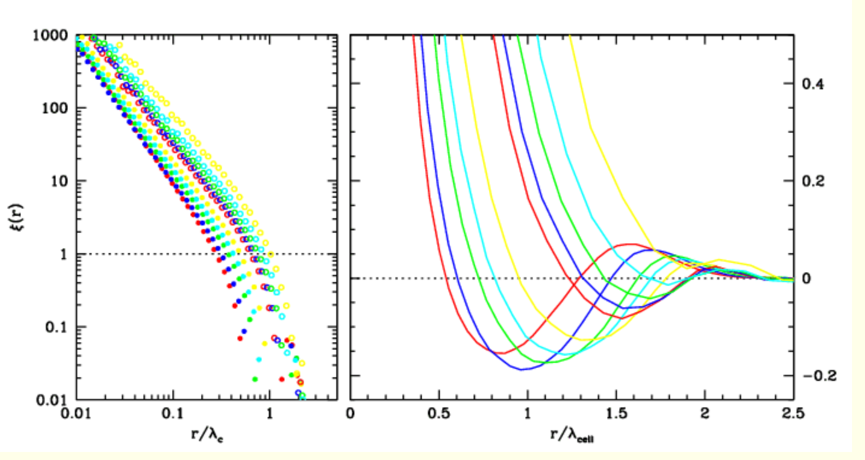

As function of mass, the correlation length r_0 and coherence length r_a increase unanimously.

Self-similar Clustering

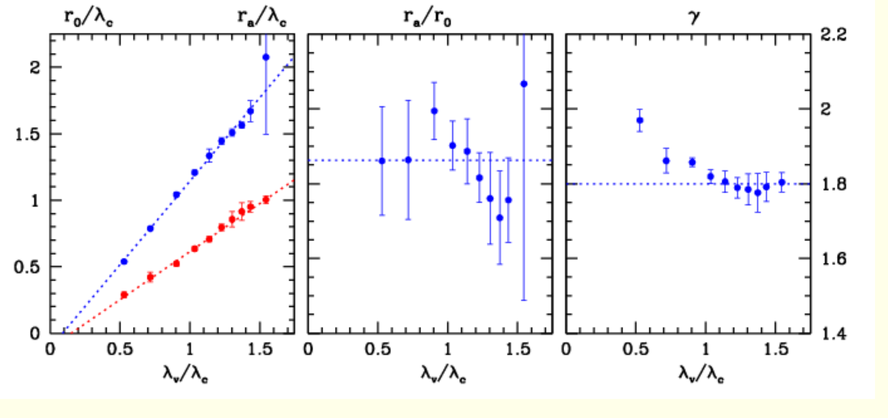

As function of mass, the correlation length r_0 and coherence length r_a increase unanimously.

Higher Order Correlation Functions:

N-point correlation functions

- N-point correlation function

$$\xi^{(n)}(\overrightarrow{x_1}, \overrightarrow{x_2}, \ldots, \overrightarrow{x_n})$$

- Probability function of finding an n-tuplet of galaxies in n specified volumes dV_1, dV_2, …, dV_n

$$\boxed{dP(\overrightarrow{x_1}, \overrightarrow{x_2}, \ldots, \overrightarrow{x_n}) = \overline{n}^n [1 + \xi^{(n)}] dV_1 dV_2 \ldots dV_n}$$

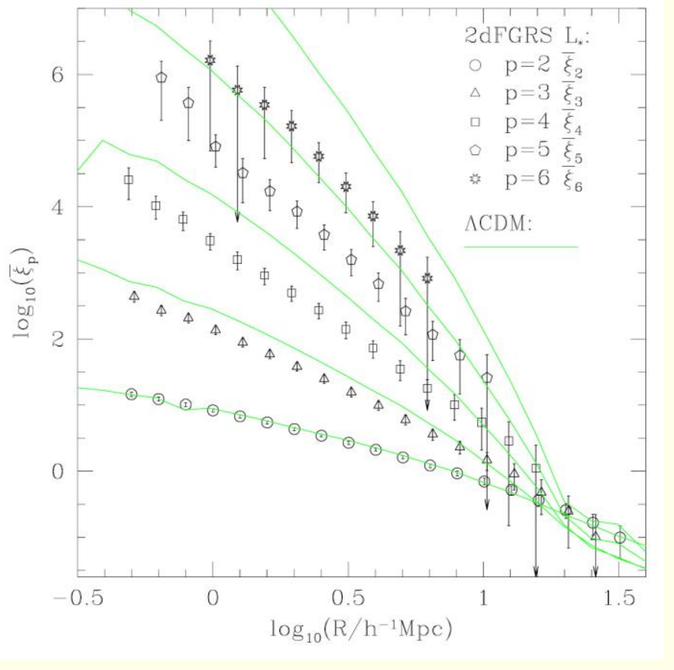

3-point correlation functions

3-point correlation function

$$dP(\vec{x}_1, \vec{x}_2, \vec{x}_3) = \bar{n}^3 [1 + \xi^{(3)}] dV_1 dV_2 dV_3$$

$$[1 + \xi^{(3)}] = \left\langle \prod_i (1 + \delta_i) \right\rangle$$

$$[1 + \xi^{(3)}] = 1 + \xi(r_{12}) + \xi(r_{13}) + \xi(r_{23}) + \zeta(\vec{r}_1, \vec{r}_2, \vec{r}_3)$$

3-point correlation functions

3-point correlation function

$$[1+\xi^{(3)}] = 1+\xi(r_{12})+\xi(r_{13})+\xi(r_{23})+\zeta(\vec{r}_1,\vec{r}_2,\vec{r}_3)$$

reduced 3-point correlation function

$$\zeta(\vec{r}_1,\vec{r}_2,\vec{r}_3) = \langle \delta_1\delta_2\delta_3 \rangle$$

excess correlation over that described by the 2-pt contributions

- $\zeta \neq 0$: non-Gaussian density field
- Hierarchical ansatz (Groth & Peebles 1977)

$$\zeta(\vec{r}_1,\vec{r}_2,\vec{r}_3) = Q(\xi_{12}\xi_{23}+\xi_{23}\xi_{31}+\xi_{31}\xi_{12})$$

Power Spectrum

Power Spectrum

- Directly measuring clustering in Fourier space:

  - More intuitive physically: separating processes on different scales
  - Theoretical model predictions are made in terms of power spectrum
  - Amplitudes for different wavenumbers are statistically orthogonal

Power Spectrum P(k)

$$\delta(\mathbf{x}) = \int \frac{\mathrm{d}\mathbf{k}}{(2\pi)^3}\, \hat{\delta}(\mathbf{k})\, \mathrm{e}^{-\mathrm{i}\mathbf{k}\cdot\mathbf{x}}$$

$$\boxed{\begin{array}{rcl} (2\pi)^3 P(k_1)\, \delta_{\mathrm{D}}(\mathbf{k}_1 - \mathbf{k}_2) & \equiv & \langle \hat{f}(\mathbf{k}_1) \hat{f}^*(\mathbf{k}_2) \rangle \\ & \Updownarrow & \\ P(k) & \propto & \langle \hat{f}(\mathbf{k}) \hat{f}^*(\mathbf{k}) \rangle \end{array}}$$

CDM Power Spectrum P(k)

$$P_{\mathrm{CDM}}(k) \propto \frac{k^n}{\left[1+3.89q+(16.1q)^2+(5.46q)^3+(6.71q)^4\right]^{1/2}} \times \frac{\left[\ln(1+2.34q)\right]^2}{(2.34q)^2}$$

$$q = k/\Gamma$$

$$\Gamma = \Omega_{m,\circ} h \exp\left\{-\Omega_b - \frac{\Omega_b}{\Omega_{m,\circ}}\right\}$$

Power Spectrum P(k)

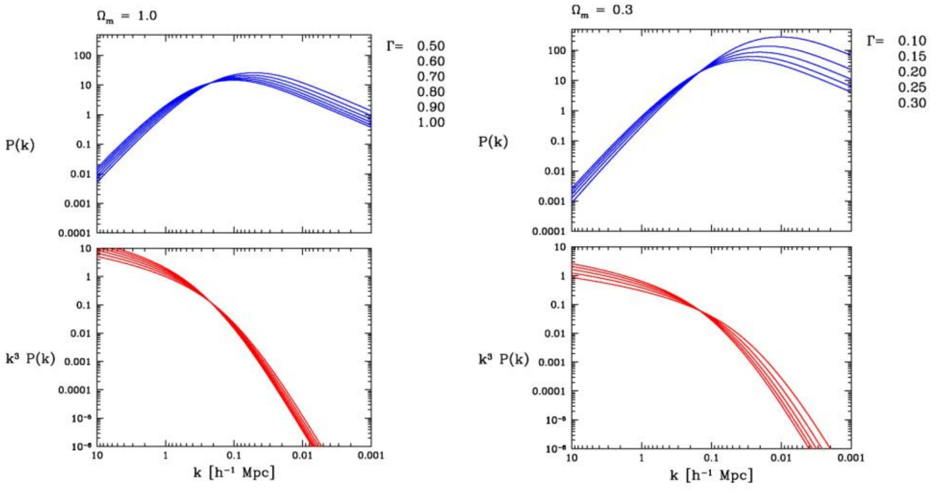

Power Spectrum - Correlation Function

$$P(k) = \int d^3 r \xi(\vec{r}) e^{i\vec{k}\cdot\vec{r}}$$

$$\xi(\vec{r}) = \int \frac{d^3 k}{(2\pi)^3} P(k) e^{-i\vec{k}\cdot\vec{r}}$$

Isotropy: $$\xi(r) = 4\pi \int_0^\infty \frac{k^2 dk}{(2\pi)^3} P(k) \frac{\sin(kr)}{kr}$$

Delta-power $$\Delta^2(k) = \frac{1}{2\pi^2} P(k) k^2$$

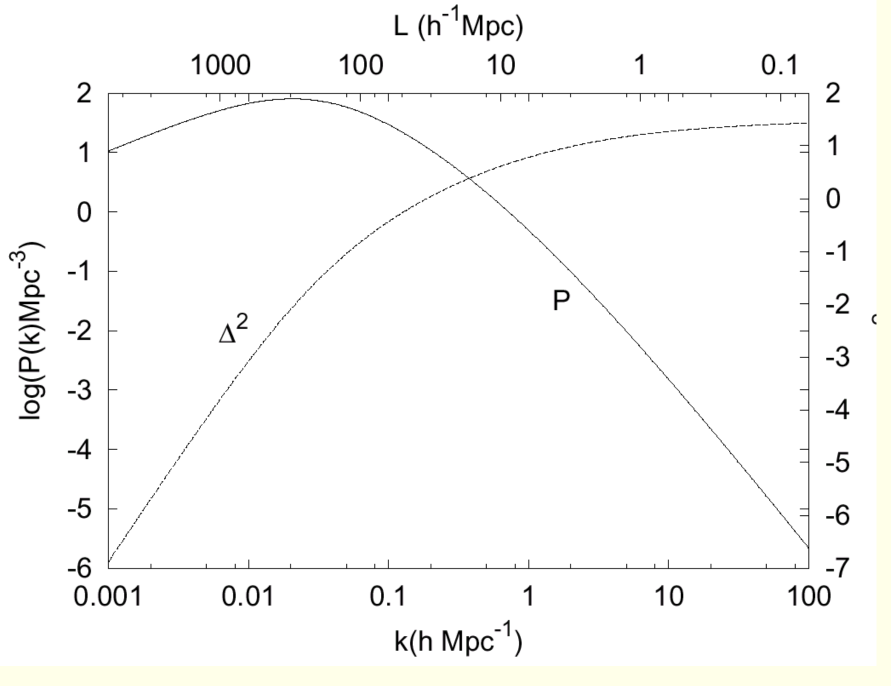

Power Spectrum Estimators

- Direct estimator
- Pixelization and maximum likelihood
- Karhunen-Loèwe (signal-to-noise) transform
- Quadratic compression
- Bayesian
- Multiresolution decomposition

Tegmark, Hamilton, Strauss, Vogeley, and Szalay, (1998), Measuring the galaxy power spectrum with future redshift surveys, ApJ, **499**, 555

Karhunen-Loeve

Decomposition in series of orthogonal
signal-noise eigenfunctions

Vogeley & Szalay 1995

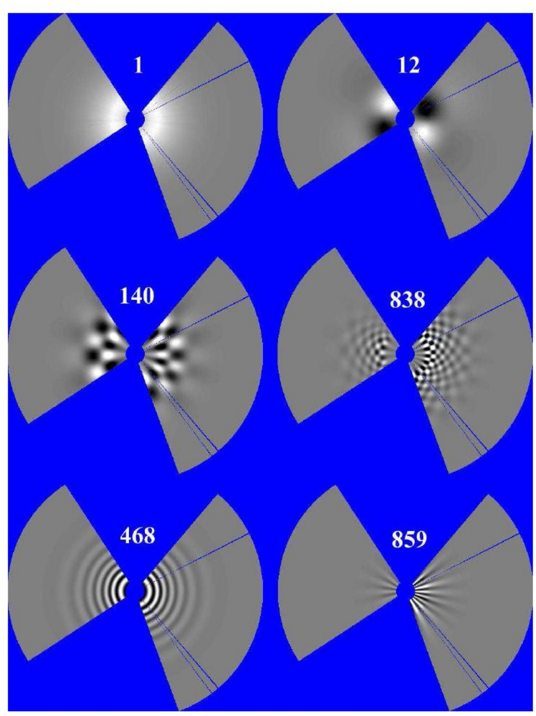

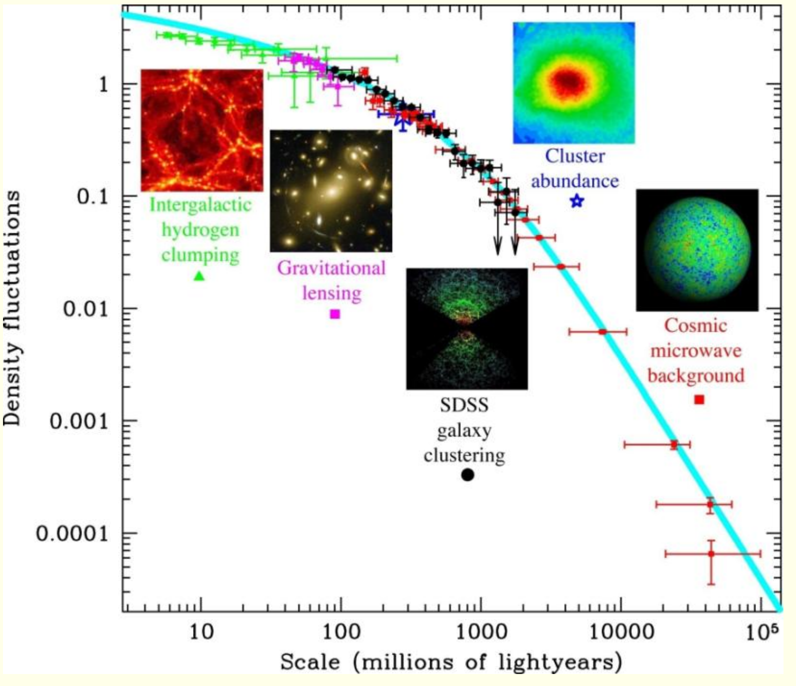

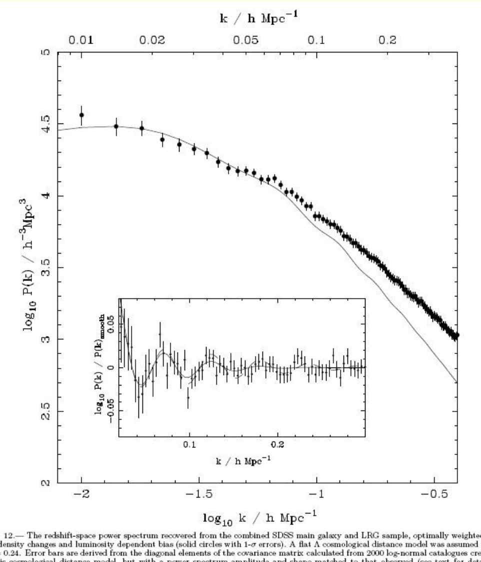

FIG. 12.— The redshift-space power spectrum recovered from the combined SDSS main galaxy and LRG sample, optimally weighted for both density changes and luminosity dependent bias (solid circles with 1-σ errors). A flat Λ cosmological distance model was assumed with $\Omega_M = 0.24$. Error bars are derived from the diagonal elements of the covariance matrix calculated from 2000 log-normal catalogues created for this cosmological distance model, but with a power spectrum amplitude and shape matched to that observed (see text for details). The data are correlated, and the width of the correlations is presented in Fig. 10 (the correlation between data points drops to < 0.33 for $\Delta k > 0.01\,h\,\mathrm{Mpc}^{-1}$). The correlations are smaller than the oscillatory features observed in the recovered power spectrum. For comparison we plot the model power spectrum (solid line) calculated using the fitting formulae of Eisenstein & Hu (1998); Eisenstein et al. (2006), for the best fit parameters calculated by fitting the WMAP 3-year temperature and polarisation data, $h = 0.73$, $\Omega_M = 0.24$, $n_s = 0.96$ and $\Omega_b/\Omega_M = 0.174$ (Spergel et al. 2006). The model power spectrum has been convolved with the appropriate window function to match the measured data, and the normalisation has been matched to that of the large-scale ($0.01 < k < 0.06\,h\,\mathrm{Mpc}^{-1}$) data. The deviation from this low Ω_M linear power spectrum is clearly visible at $k \gtrsim 0.06\,h\,\mathrm{Mpc}^{-1}$, and will be discussed further in Section 6. The solid circles with 1σ errors in the inset show the power spectrum ratioed to a smooth model (calculated using a cubic spline fit as described in Percival et al. 2006) compared to the baryon oscillations in the (WMAP 3-year parameter) model (solid line), and shows good agreement. The calculation of the matter density from these oscillations will be considered in a separate paper (Percival et al. 2006). The dashed line shows the same model without the correction for the damping effect of small-scale structure growth of Eisenstein et al. (2006). It is worth noting that this model is not a fit to the data, but a prediction from the CMB experiment.

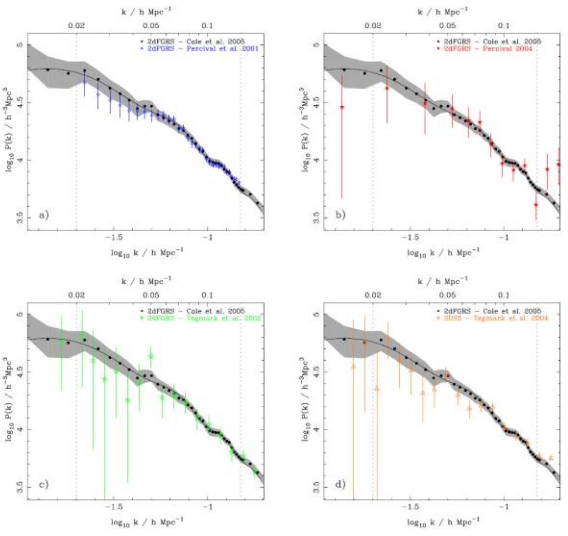

Figure 16. The redshift-space power spectrum calculated in this paper (solid circles with 1σ errors shown by the shaded region) compared with other measurements of the 2dFGRS power-spectrum shape by (a) Percival et al. (2001), (b) Percival (2005), and (c) Tegmark et al. (2002). For the data with window functions, the effect of the window has been approximately corrected by multiplying by the net effect of the window on a model power spectrum with $\Omega_m h = 0.168$, $\Omega_b/\Omega_m = 0.0$, $h = 0.72$ & $n_s = 1$. A zero-baryon model was chosen in order to avoid adding features into the power spectrum. All of the data are renormalized to match the new measurements. Panel (d) shows the uncorrelated SDSS real-space $P(k)$ estimate of Tegmark et al. (2004), calculated using their 'modelling method' with no FOG compression (their Table 3). These data have been corrected for the SDSS window as described above for the 2dFGRS data. The solid line shows a model linear power spectrum with $\Omega_m h = 0.168$, $\Omega_b/\Omega_m = 0.17$, $h = 0.72$, $n_s = 1$ and normalization matched to the 2dFGRS power spectrum.

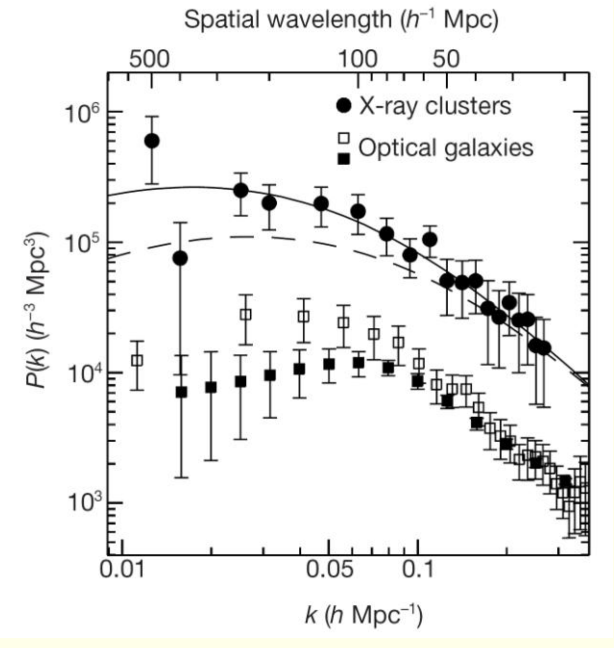

Minimal Spanning Tree

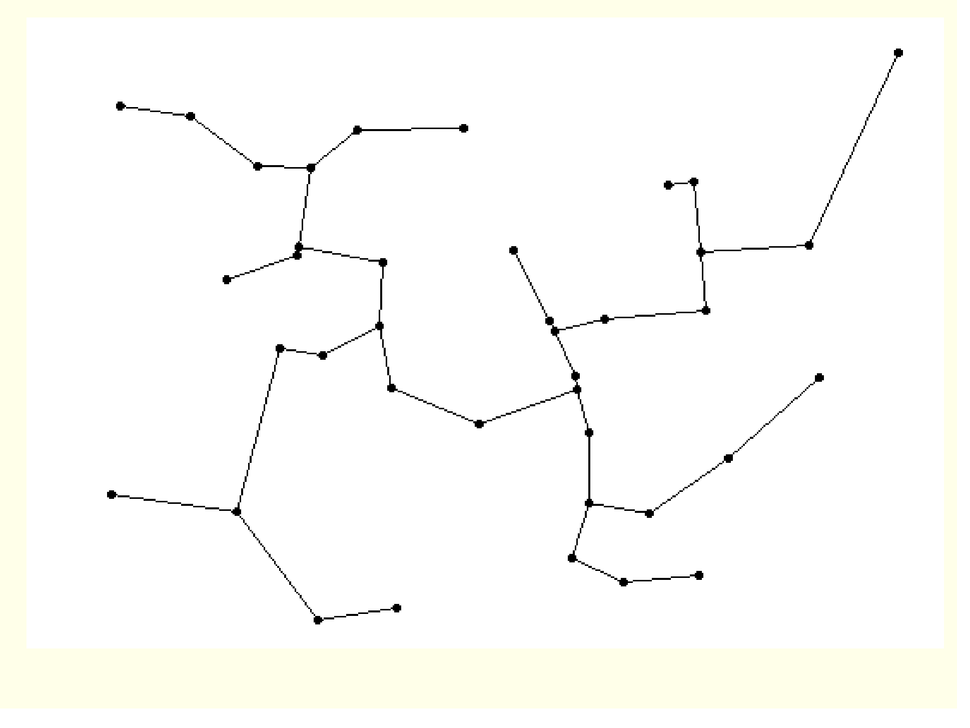

Topology

Topology and the Morphology of LSS

- Deals with *Excursion Sets*, i.e. regions where a field exceeds a certain level usually given in terms of the *rms* fluctuation.
- This could be the temperature field on the CMB Sky or the density field traced by galaxies.
- In general the excursion set will consist of a number of disjoint pieces which may be simply or multiply connected.

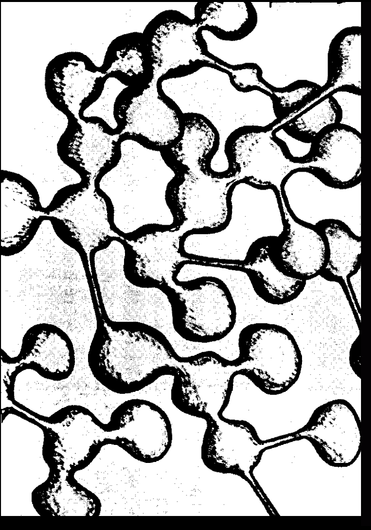

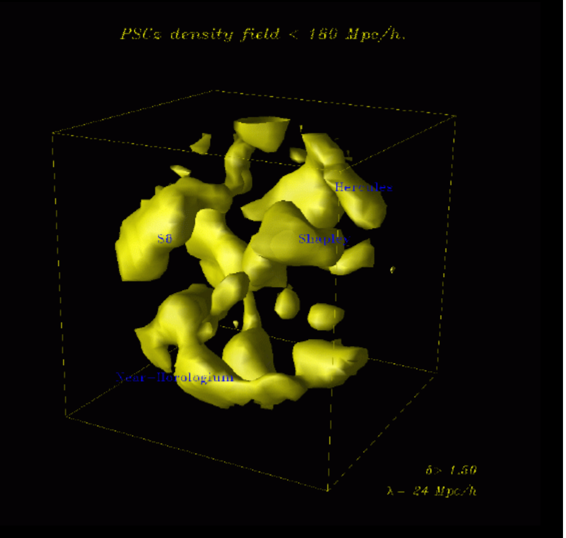

The Gauss-Bonnet Theorem

$$\boxed{2\pi\chi(M) = \int_M k\,dA + \int_{\partial M} k_g\,ds + \sum_{i=1}^{n}(\pi - \alpha_i)}$$

Two dimensional manifold M with boundary ∂M; k is the Gaussian curvature of M; k_g is the geodesic curvature of ∂M; the boundary is piecewise smooth, having *n* vertices

The quantity χ is the Euler-Poincaré characteristic of M and is a topological invariant…

Topology in 2D

For a 2D excursion set defined on a flat plane,

$$2\pi\chi = \int k_g ds = \int \frac{ds}{R_1 R_2}$$

In 2D, this gives the *number of isolated regions minus the number of holes in such regions*..

Lots of isolated regions: χ>0, like “meatballs”

One isolated region with lots of holes: χ<0, like “Swiss cheese”

The Usefulness of χ

The mean value of χ can be calculated analytically for Gaussian random fields (test of GRF hypothesis?)

In 3D the mean level is characterised by g>0 (a sponge)

In 2D the mean level has χ=0.

There is no 2D equivalent of a sponge!

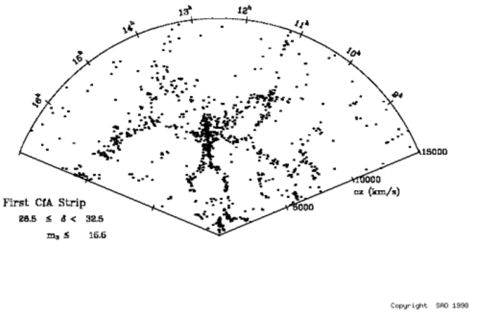

Topology in 3D

For a 3D excursion bounded by a 2D surface

$$2\pi\chi = \int k \; dA = 4\pi(1-g)$$

In 2D, it is typical to refer to the *genus, g,* which is the number of "handles"

g=0

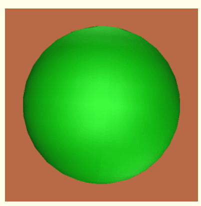

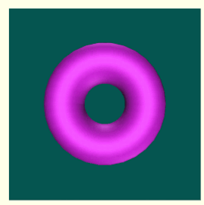

g=1

Topological Genus

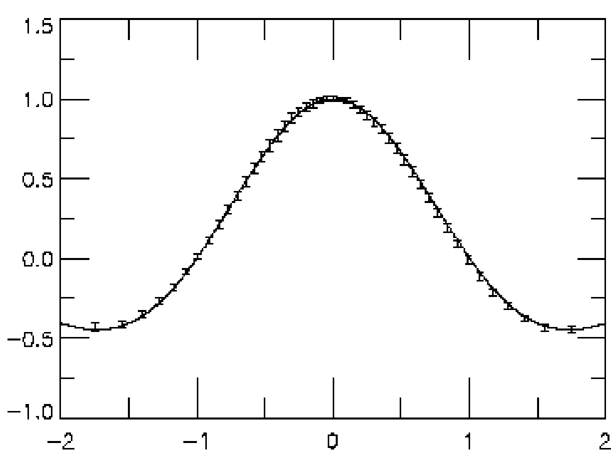

FIG. 3.— The average genus curve for 50 realizations of a Gaussian random field with $P(k) =\sim k^{-1}$ together with the expected analytical result (solid line). Error bars are 1 σ deviations.

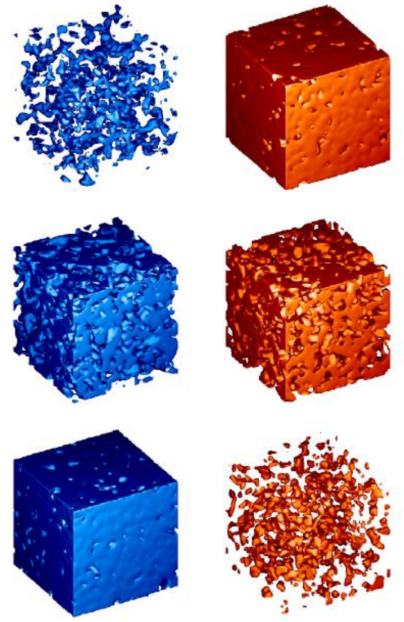

FIG. 1.— Spatial distribution of the low- (left column) and high density (right column) regions for a realization of a Gaussian random field, with comparatively little smoothing. The upper pair shows the 7% low, 93% high density regions, the middle pair stands for 50%–50%, and the lower pair shows the 93% low-density, 7% high-density case.

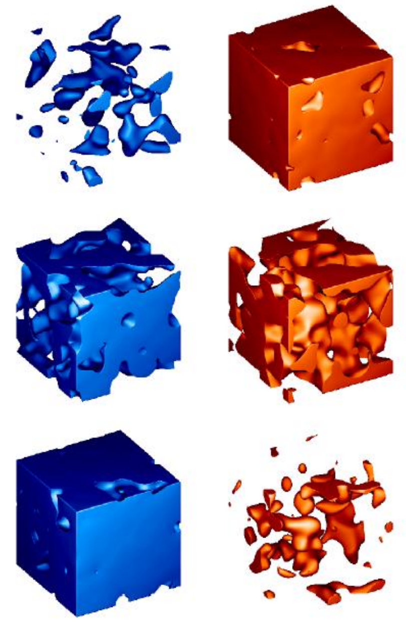

FIG. 2.— Spatial distribution of the low- (left column) and high density (right column) regions for a realization of a Gaussian random field, with heavy smoothing. The upper pair shows the 7% low, 93% high density regions, the middle pair stands for 50%–50%, and the lower pair shows the 93% low-density, 7% high-density case.

Minkowski functionals

- More recently this has been put on a much more rigorous footing using Minkowski functionals.
- In d dimensions there are (d+1) invariants satisfying additivity, continuity, translation invariance and rotation invariance.
- In 3D, for example, these are:

  volume,
  area,
  mean curvature,
  Euler-Poisson characteristic χ

Minkowski functionals in 2D (area, length and χ)

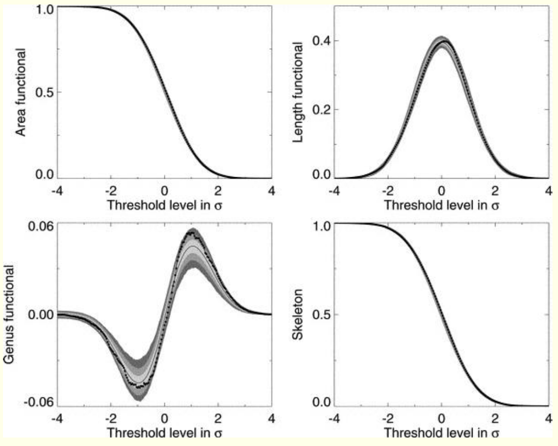

Minkowski functionals

In R^3 four functionals:

volume V
surface area A
integral mean curvature H
Euler-Poincare characteristic χ

The are the Minkowski Functionals

Kerscher & Martínez (1998), Bull. Int. Statist. Inst. 57-2, 363

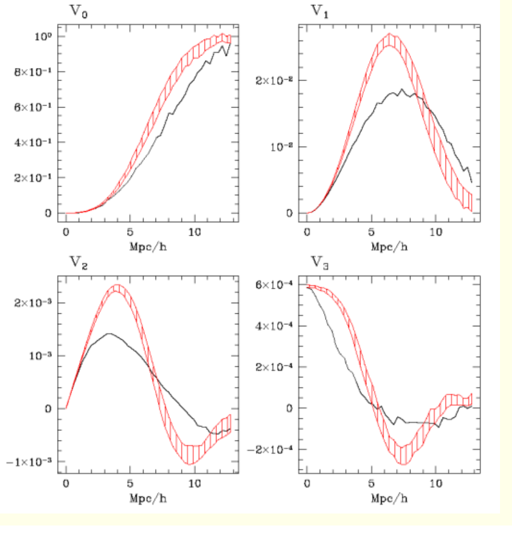

Morse Theory

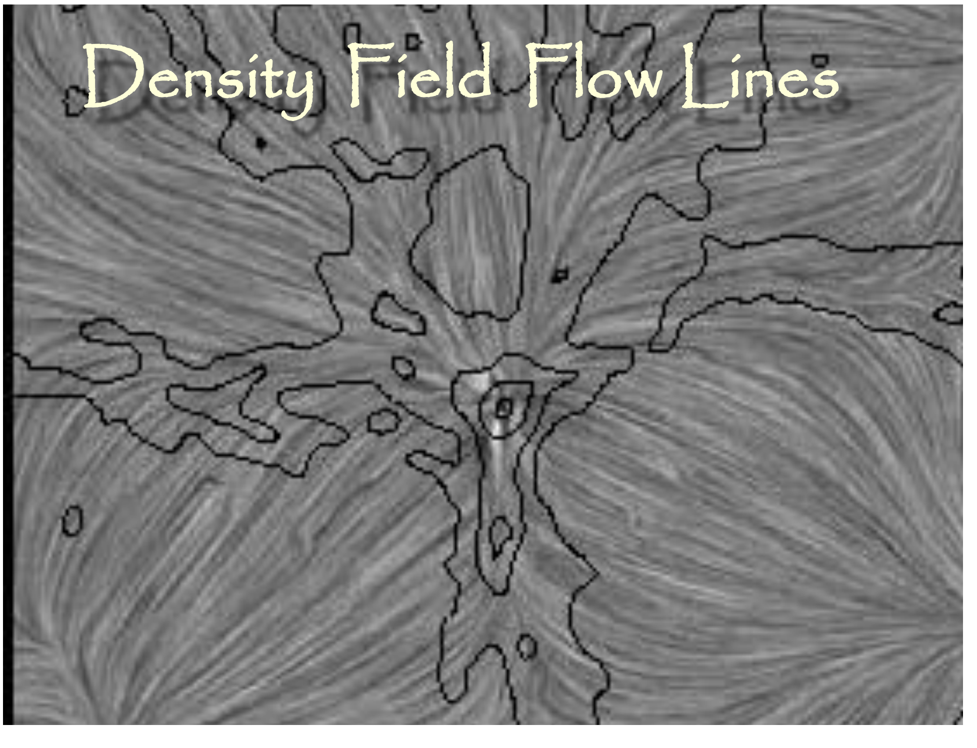

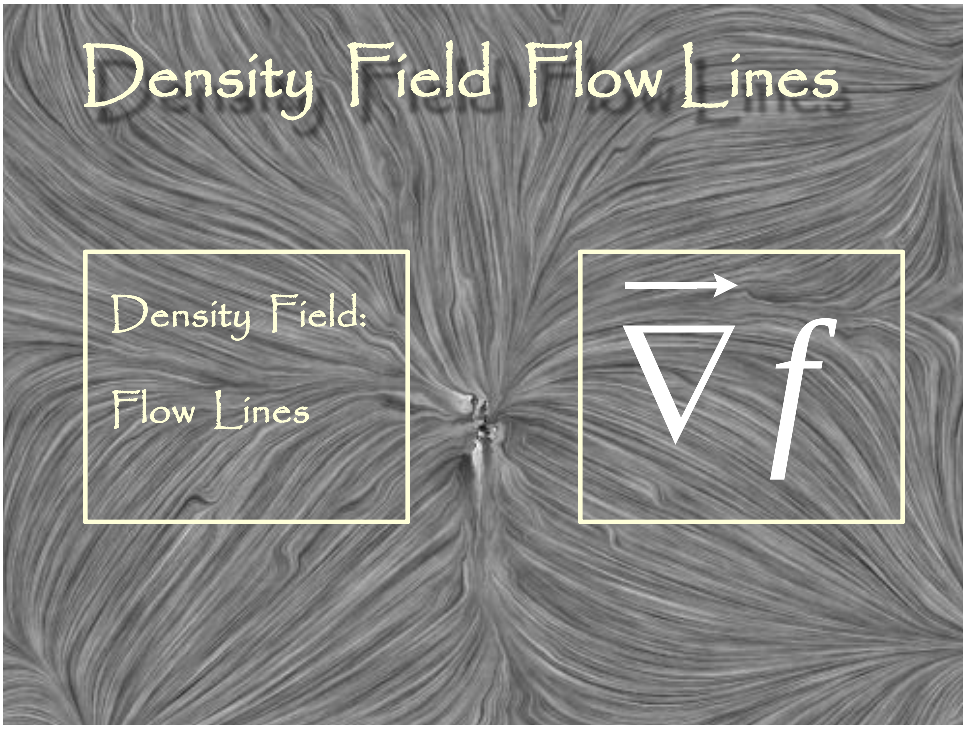
Density Field Flow Lines
Density Field:
Flow Lines
$\vec{\nabla} f$

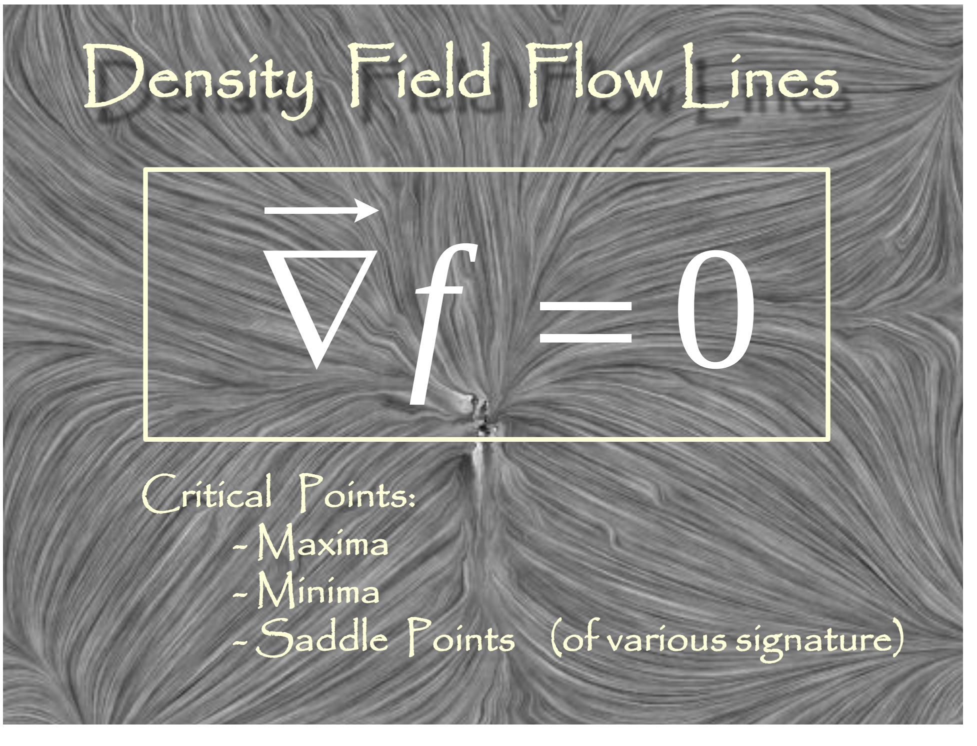
Density Field Flow Lines
$\vec{\nabla} f = 0$
Critical Points:
- Maxima
- Minima
- Saddle Points (of various signature)

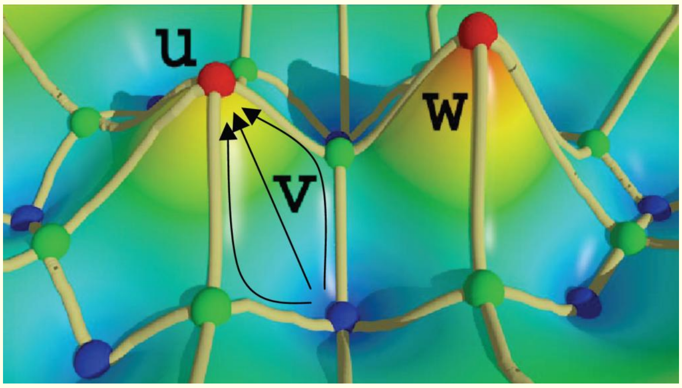

Density Field
Critical Points:

Ridges:

Connections
Saddle-
Maxima

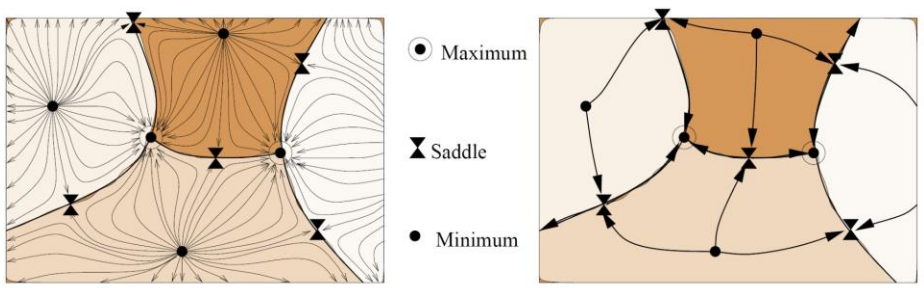

Integral Lines & Field Ridges:

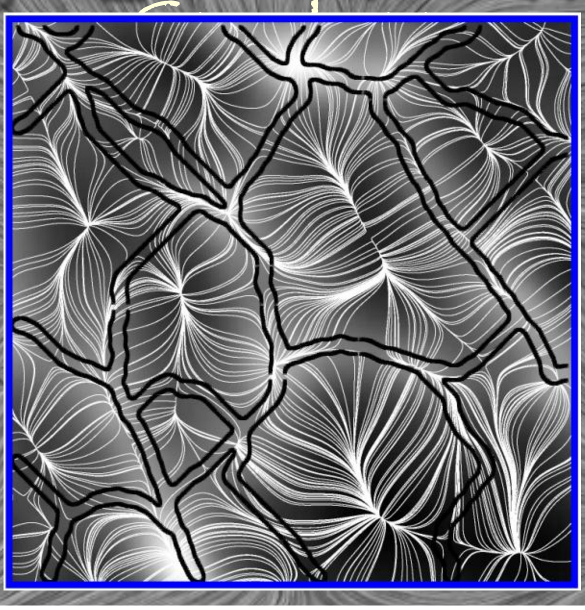

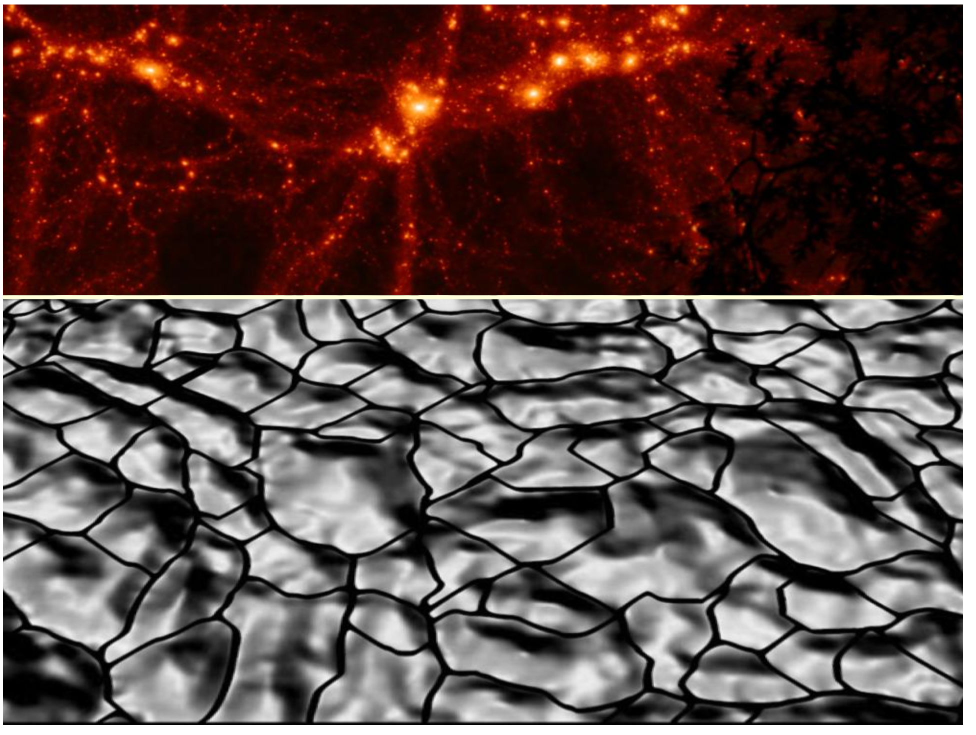

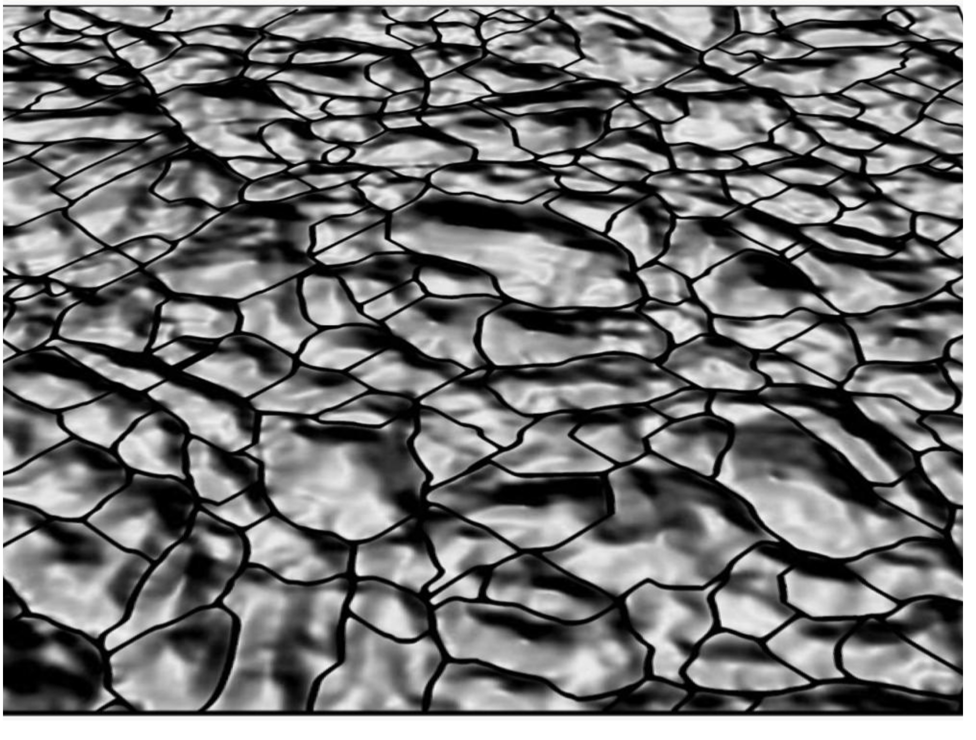

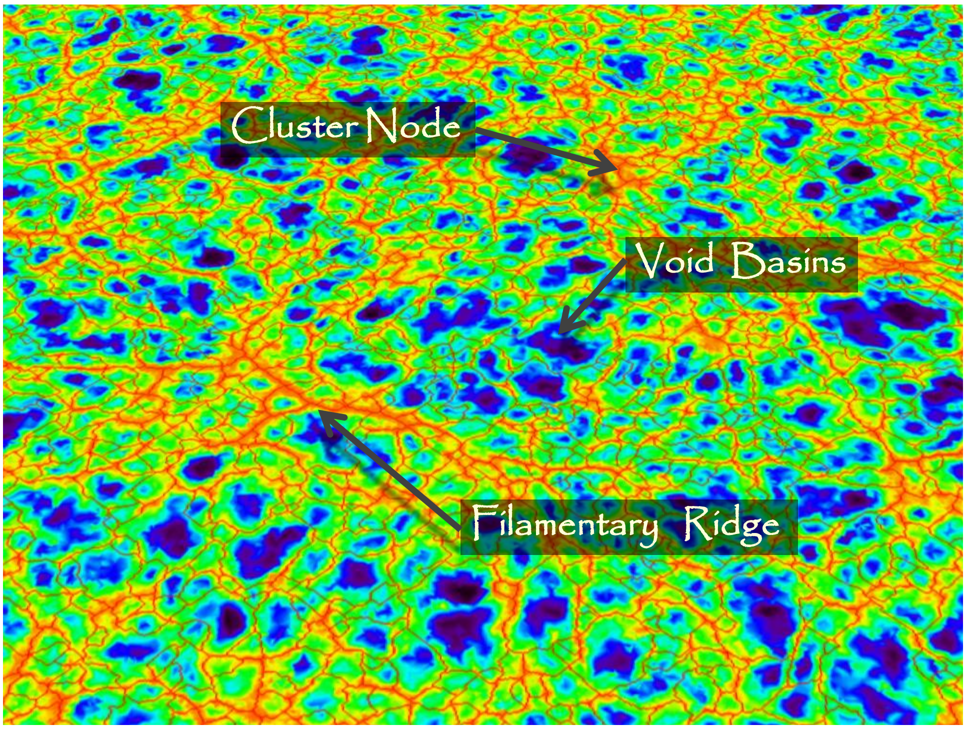
Cluster Node
Void Basins
Filamentary Ridge

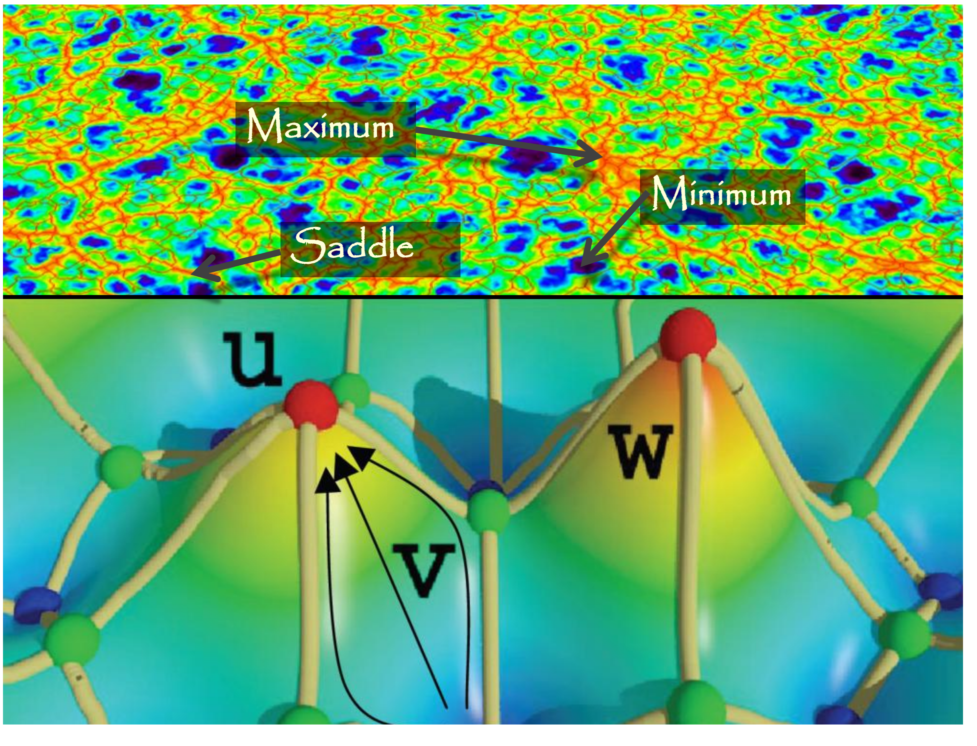
Maximum
Minimum
Saddle
u
w
v